Investigation of Iron Oxide Reduction by TEM

MANN-FU RAU, DAVID RIECK, and JAMES W. EVANS

An "environmental cell" located in a high voltage transmission electron microscope has been used to study the reduction of single crystal iron oxides by hydrogen and hydrogen-argon mixtures. The cell enables a direct observation of the solid during reaction, thus permitting the nucleation and growth of solid reaction products to be observed. Hematite was reduced at temperatures in the range 387 to 610 °C with gas pressures up to 5.3 kP. Reduction with pure hydrogen was considerably faster than when argon was present. Lath magnetite which rapidly transforms to porous magnetite and thence (more slowly) to porous iron was observed. The reduction of magnetite and of wustite single crystals was observed in the temperature range 300 to 514 °C using both hydrogen and hydrogen-argon mixtures at gas pressures up to 6.6 kP. Incubation periods were found for magnetite reduction; during these periods faceted pits formed in the oxide. Iron formed in the early stages was epitaxial with the host magnetite; at later stages the epitaxy was lost and fissures frequently formed in the metal. The morphology of the iron differed between the gas mixtures. Disproportionation accompanied the reduction of wustite, producing intermediate polycrystalline magnetite despite reducing conditions. The disproportionation appeared to be promoted by the reduction reaction. For both oxides, reduction in the hydrogen-argon mixture was slower than in pure hydrogen.

I. INTRODUCTION AND PREVIOUS INVESTIGATIONS

THE reduction of iron oxides by hydrogen or carbon monoxide (or their mixtures) is one of the most frequently studied topics in extractive metallurgy. The reader is referred to reviews[1-4] for a detailed account of research carried out on a macroscopic scale; that is, on pellets, sinter, or lump ore such as are fed to the iron blast furnace or a direct reduction unit. The present investigation is concerned with microstructural aspects of iron oxide reduction, in particular the nucleation, growth, and morphology of second solid phases on a scale of micrometers.

Macroscopic studies of iron oxide reduction at temperatures encountered in industrial processes have frequently led to the conclusion that pore diffusion of gases is rate controlling, except for small particles (*e.g.*, References 9, 10). The pore diffusion of gases referred to here is the diffusion of gaseous reactants and products through porous reactant or product. The pore structure (porosity, pore size distribution) is therefore of significance in determining the reaction rate under conditions of pore diffusion or mixed controlled. Turkdogan *et al.*[11] have shown that the structure of the porous iron formed on reduction is very dependent on reduction temperature, being coarser at higher reduction temperature. Koo and Evans[12] showed that the structure of porous iron ores can be markedly altered by holding at temperature prior to reduction. An important microstructural aspect of iron oxide reduction is therefore the development of porosity in solid reaction products.

Edstrom[13] and Edstrom and Bitsianes[14] used optical microscopy to study the relation between microstructure and reduction rate. They observed that the reduction of hematite occurred more rapidly when there was early and extensive formation of pores in the solid reaction products. Brill-Edwards *et al.*[15] studied the reduction of polycrystalline hematite and observed randomly distributed spherical pores for reduction temperatures between 400° and 700 °C with elongated pores between 700° and 900 °C.

A second microstructural aspect of iron oxide reduction is the nucleation and growth of the solid reaction products. A recent paper on the reduction of wustite is that of El-Rahaiby and Rao.[5] These investigators used polycrystalline specimens of wustite about 50 μm in thickness and carried out hydrogen reduction at 238 to 417 °C. They observed a sigmoidal relationship between extent of reaction and time. That is, on contacting the oxide with the gas there was an initial "incubation" period where little reaction took place, followed by an intermediate period of accelerating reaction rate with a final period of slowing rate. The occurrence of such incubation (or "induction") periods, particularly at lower temperatures, has been noted by many other investigators for both iron oxide reduction and other gas-solid reactions.[12] A frequent explanation is that the incubation period is due to the nucleation and growth of the second solid phase (iron in the case of wustite reduction). Rao and co-workers[6,7,8] have recently studied the reduction of magnetite and hematite by similar techniques.

Pluschkell and Yoshikoshi[16] and Rao[17] have used hot stage optical microscopes in investigations of wustite reduction. With these microscopes the growth of iron was directly observable under reaction conditions. Bradshaw and Matyas[18] used mercury penetration porosimetry and conventional optical microscopy in a study of the reduction of hematite pellets to magnetite. They suggested that formation of magnetite nuclei could be rate limiting.

St. John and Hayes[19] have used scanning electron microscopy to examine wustite specimens at various stages of reduction by hydrogen or H_2/H_2O mixtures at temperatures from 600 to 1000 °C. Faceted pits were observed prior to nucleation of iron when wustite was reduced with 1 atm pure hydrogen at 1000 °C. At temperatures below 900 °C, pit formation was less pronounced. They noted that pores in the iron product were generally larger as the reducing gas composition approached that of the Fe/FeO equilibrium.

MANN-FU RAU is Materials Engineer, Morgan Semiconductor, 2623 National Circle, Garland, TX 75041. DAVID RIECK is with the Department of Animal Science, South Dakota State University, Brookings, SD 57006. JAMES W. EVANS is Professor and Chairman, Department of Materials Science and Mineral Engineering, University of California, Berkeley, CA 94720.

Manuscript submitted November 21, 1985.

St. John and co-workers[36] have recently reported different results for the reduction of wustite with CO/CO_2 mixtures; the effect of temperature on the product morphology was much less pronounced in this case. However, the porosity of the iron formed was dependent on the CO content of the reducing gas. Contrary to the case of hydrogen reduction, these investigators observed iron whiskers on reduction in CO/CO_2 mixtures. They determined that a dense iron layer formed on the surface initially and that, under conditions where porous iron formed, it did so by breakdown of this initial dense layer. St. John *et al.*[37] developed a model for the breakdown of the dense iron layer; the model involved rupturing of the iron layer by gas formed at the iron-oxide interface.

Moukassi *et al.*[20] have shown that the "rate minimum" (a minimum in reaction rate on increasing the reduction temperature), observed in many macroscopic studies of iron oxide reduction, is connected with the evolution of the iron structure toward a dense layer of metal that acts as a barrier to the diffusion of gas.

Some of the investigations cited above have been concerned with the microstructure of iron produced by reduction. In the case of hematite reduction, magnetite is an intermediate reaction product and the microstructure of the magnetite may have a significant effect on the kinetics of the hematite reduction and the subsequent magnetite reduction. Many investigators[15,21-25] have reported the occurrence of two kinds of magnetite, porous magnetite and dense "lath magnetite", the formation of the latter being favored at high temperatures. Swann and Tighe[23] reported that lath magnetite could act as a nucleus for the growth of porous magnetite but that porous magnetite could also be formed without prior formation of lath magnetite.

The electron microscope provides a convenient means for study of microstructural aspects of gas-solid reactions and has been used in several of the investigations referred to above. With the exception of the work of Swann and collaborators,[23,24] all such investigations have made *ex situ* examinations of the solid specimens. In this method specimens are exposed to the reactive gas at temperature and then withdrawn from that environment to be placed in the electron microscope. The method has the disadvantage that structural changes, or even reaction, can occur as the specimen is cooled and transferred to the microscope. Even if the rapid quenching procedure, described by Hayes and coworkers,[19] is used there exists the possibility that the microstructure seen in the microscope differs from that under reaction conditions. Furthermore, although a specimen can usually be returned to the reaction apparatus, enabling the microstructure of the specimen to be examined at various stages in the reaction, it is frequently difficult to relocate the same region of the specimen because of obliteration of recognizable features of the specimen as reaction proceeds. A technique for overcoming this difficulty in *ex situ* studies has been described by Little *et al.*[26]

The alternative to *ex situ* studies is the use of an "environmental cell" within the electron microscope. Studies with such a device (described more fully below) are *in situ* investigations or are frequently referred to by the acronym CAEM (controlled atmosphere electron microscopy). The technique has been employed to study reactions in scanning electron microscopes (*e.g.*, References 27, 28), but of interest in the present investigation is its use in transmission electron microscopy. *In situ* studies of gas-solid reactions have included investigations of carbon gasification,[29,30,31] chemical vapor deposition reactions,[32] oxidation of gallium arsenide,[33] and the thermal decomposition of ammonium salts.[34] Swann and co-workers[23,24] have made considerable use of the *in situ* technique in their study of the reduction of hematite to magnetite in H_2-He and CO-CO_2 mixtures. The present investigation has used the technique to study other iron oxide reduction reactions.

II. EXPERIMENTAL APPARATUS AND PROCEDURE

Most of the microscopy of this investigation was carried out on the Hitachi HU-650 transmission electron microscope at Lawrence Berkeley Lab. Occasional use was made of the Kratos EM-1500 electron microscope at the same location. Both microscopes have environmental cells (Gatan Co.) with hot stages and a single tilt axis.

The environmental cells were equipped with small electric furnaces. Calibration curves of furnace temperature *vs* current were determined in the various gas environments used in this investigation. The accuracy of the heater and thermocouple was tested using two TEM samples made of 6 pct Cu-94 pct Al. The TEM specimens were heated until the phase precipitates disappeared. The precipitates disappeared in one specimen at 552 °C; in the other specimen the precipitates disappeared at 560 °C. Aluminum alloys with 6 pct Cu are single phase at temperatures above 548 °C. From the above tests it is seen that temperatures within approximately 10 °C of the measured temperature can be achieved.[38]

Gas from a cylinder flowed *via* a regulator, flowmeter (Hastings NALL-500), and valves to the environmental cell. Pressure was measured at a point just before the gas entered the cell using a SPEEDVAC pressure gage (Edwards High Vacuum Type C.G.3).

Wustite single crystals used in this investigation were obtained from Purdue University and were prepared by skull melting.[35] Magnetite single crystal slab was prepared by Argonne National Lab. Hematite single crystal was available at Lawrence Berkeley Lab but of unknown source. The hematite sample was subjected to spectrographic analysis and showed a few impurities at the level of a few tens of parts per million. Gases used in the investigation were obtained from Lawrence Berkeley Lab. A mass spectrometer was used to check the impurity levels of some gas cylinders; only trace amounts of impurities were found.

Specimens of oxides were prepared by diamond sawing, grinding (#600 silicon carbide paper) and polishing (6 μm followed by 1 μm diamond paste) to a thickness of approximately 50 μm. Final thinning was by means of an ion mill (with a cold stage in the case of wustite specimens).

After loading a specimen into the environmental cell and pumping down the microscope, electron images of the initial specimen were taken. Thereafter the flow of gas from the gas supply was commenced and time allowed for purging of gas lines and the establishment of stable pressures (approximately ten minutes). The heater current was then switched on and set to the required value; the reaction temperature was achieved typically in less than ten seconds. Photomicrographs were taken as the reaction proceeded. Reaction

was halted (by turning off the power) after only partial reaction because of the danger of porous reaction products falling apart. Some specimens were examined subsequent to reduction; such *ex situ* examinations permitted a more complete structural analysis than was possible *in situ*.

III. RESULTS AND DISCUSSION

A. *Hematite Reduction*

Swann and co-workers[23,24] have studied the reduction of hematite, but their published results are confined to the reduction to magnetite. The present investigation is concerned with this reduction and the subsequent reduction to iron.

Reduction with pure hydrogen

Figure 1 shows the appearance of an edge of the sample before and after exposure to 270 P of pure hydrogen at 387 °C for 220 seconds. Little or no reaction was observed in the first 150 seconds and thereafter reaction was observed to proceed rapidly. This is consistent with results from macroscopic studies of hematite reduction where an incubation period is reported.[22] The dark lines paralleling the edge of the specimen in the upper figure are thickness contours arising from the tapering of the specimen toward its edge. The small dark grains in this micrograph were identified from the electron diffraction pattern as magnetite that may have been formed during ion thinning. This amount of magnetite is small and, as will be seen below, is unlikely to have affected the reaction.

Figure 2(a) is the electron diffraction pattern for the central region of Figure 1 after 220 seconds exposure to hydrogen. The "spotty" ring pattern corresponds to polycrystalline

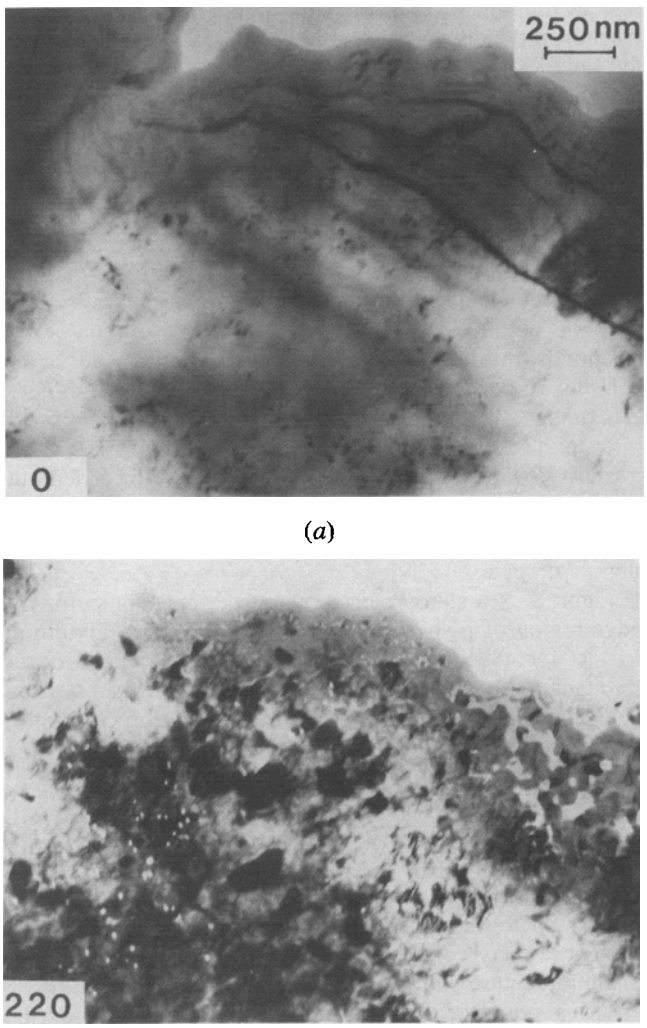

(*a*)

(*b*)

Fig. 1—Electron micrographs of hematite specimen before (*a*) and after (*b*) reducing in 270 P pure hydrogen at 387 °C for 3 min and 40 sec. The product phases include porous iron (right), polycrystalline magnetite (center), and pores (left).

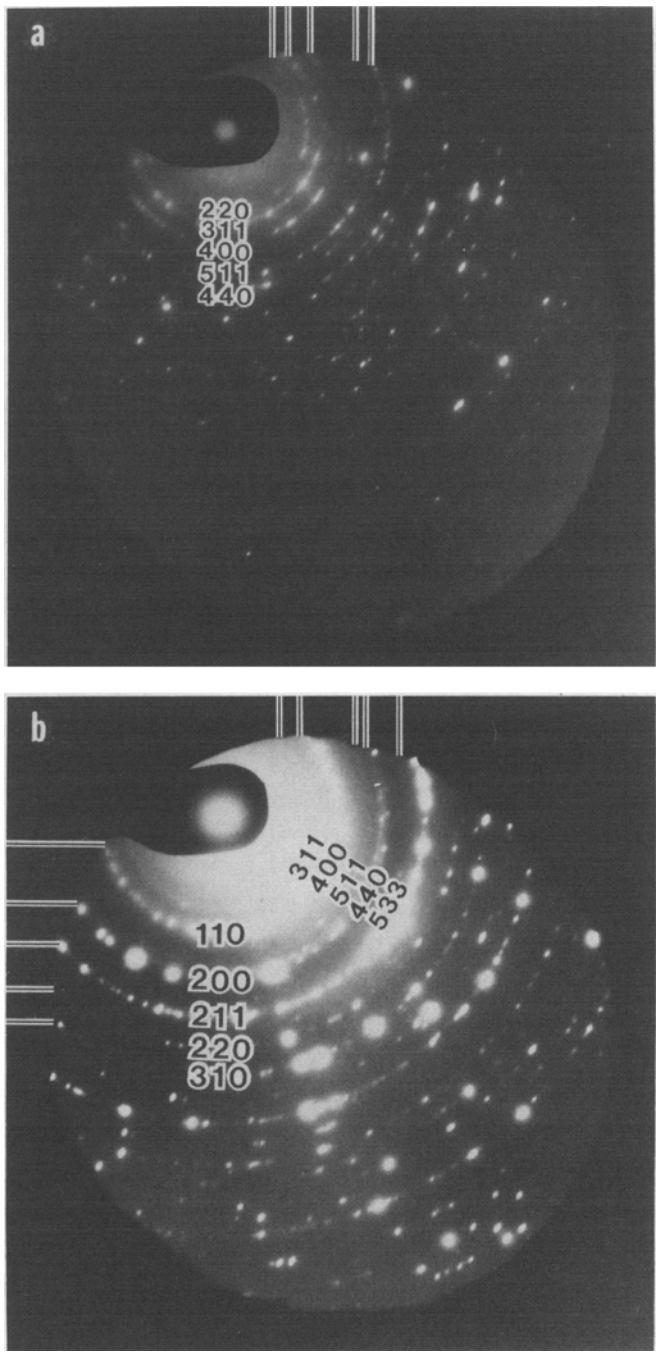

Fig. 2—Typical electron diffraction pattern for (*a*) the center part of the region in Fig. 1 showing that only polycrystalline magnetite exists, and (*b*) to the right of the region revealing that porous iron coexists with polycrystalline magnetite.

magnetite. Figure 2(b) is the diffraction pattern for a region to the right of Figure 1 and reveals the presence of polycrystalline iron. This region of the edge of the specimen was the point at which reaction was seen to start and sweep through the volume of the specimen.

An (*ex situ*) overview of a whole reaction zone after 880 seconds is presented as Figure 3; this is a region not previously struck by the electron beam. The dark band is lath magnetite separating the inner porous mass of magnetite and iron from unreacted single crystal hematite. The minute black grains on the hematite are those initially present that were mentioned above; they have not become sites for reaction. Figure 3 creates an impression of "topochemical" reaction such as is frequently observed in macroscale studies of gas-solid reactions. It should be noted, however, that, because the specimen is a thin foil, reaction is starting at an edge rather than on the surface, and subsequently propagating through the body of the sample.

Figure 4 shows the diffraction patterns from various regions of Figure 3. The diffraction patterns were taken with a 500 nm aperture centered about the points indicated by the lines. Region (a) is identified as iron, while the other three regions have the diffraction pattern corresponding to magnetite. A schematic diagram of a cross section of the foil appears as Figure 5. Region I is predominantly porous iron; in regions II and III porous magnetite is the predominant phase and the shrinkage resulting from the lower volume of magnetite (compared to hematite on a per mole of iron basis) results in this region having high porosity. Region IV has lower apparent porosity due to residual hematite. It is conjectured that the lack of porosity of the lath magnetite may be a consequence of this phase existing as thin sheets that can accommodate the volume change by transverse shrinkage.

In their *ex situ* studies of hematite reduction, Swann and Tighe noted that porous magnetite is the product of hematite reduction at temperatures below 650 °C and that lath magnetite results from reduction above 850 °C. Baguley *et al.*[25] noted that lath magnetite was observed in the initial stages of reduction at 400 °C and that the lath magnetite acted as nucleation sites for subsequent growth of the porous magnetite.

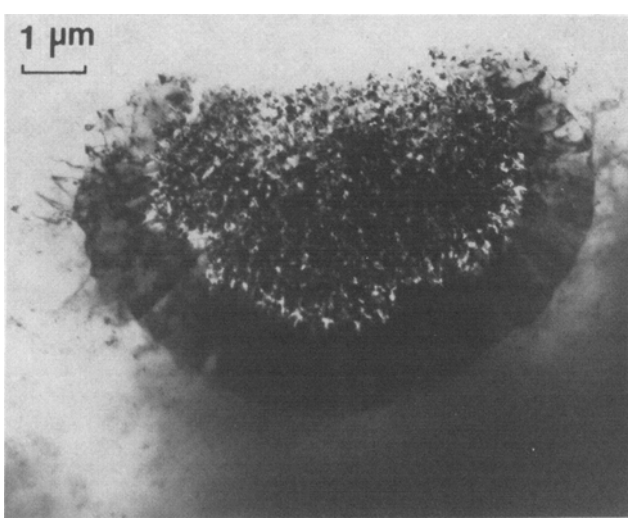

Fig. 3—Typical configuration of reaction zones after hematite reduction using pure hydrogen. The specimen was reduced by 270 P H_2 at 387 °C for 14 min and 40 sec.

The reaction fronts were seen to slow down as they moved into thicker regions of the sample. The width of the layer of lath magnetite stayed constant at approximately 1 μm. This suggests that lath magnetite is a short lived intermediate in the reduction and that the formation of lath magnetite from hematite and its transformation to porous magnetite are not rate controlling; the slow reduction of porous magnetite to iron is indicated by the large amount of porous magnetite observable in micrographs such as Figure 4. This confirms the results of Rao and Moinpour[6] who studied reduction of hematite with pure hydrogen in the temperature range 245 to 482 °C and noted that the rate controlling step appears to be the conversion of magnetite to iron.

There is a possibility of the reduction reactions being affected by the presence of the electron beam, perhaps as a consequence of heating of the specimen by the beam or because of radiation damage. Initiation of reaction always occurred in a region of the hematite struck by the beam although it also occurred in other regions. Advancement of the reaction fronts appeared to proceed more rapidly in the regions illuminated by the beam, but the morphology of the reaction products was not significantly affected. None of the samples examined showed evidence of wustite formation during reduction which is consistent with the thermodynamic instability of this oxide below 570 °C.

At the temperatures employed in this investigation little change occurs in the structure of the porous iron product. Figure 6 shows a region that is predominantly iron 3 minutes (a) and 14 minutes (b) after the original hematite was contacted with 270 P of hydrogen at 417 °C. Note that the morphology changes little in the 11-minute interval except near the point X where some enlargement of pores and reaction of residual magnetite is discernible.

Using 10 pct H_2/90 pct Ar as reducing gas, preliminary experiments were carried out using temperatures and pressures in the ranges employed with pure hydrogen. Reaction was too slow and subsequent experiments were carried out at 5.3 kP total pressure and higher temperatures. Even then, hematite reduction was much slower than observed using pure hydrogen.

Figure 7 is a stereo pair showing the appearance of the edge region of a specimen exposed to this gas mixture at 610 °C for 480 seconds. Reaction was observed to occur throughout the volume of the specimen, rather than starting at an edge and sweeping through the volume, in contrast to reduction in pure hydrogen. Examination of Figure 7 with a stereo viewer reveals that there are no pores present.

Figure 8 shows bright-(a) and dark-(b) field images of magnetite produced by 10 minutes exposure at these conditions. Diffraction patterns (c) and (d) were taken from the center and tip of the region shown in Figure 8(a). The diffraction patterns reveal that neither iron nor wustite is present in the specimen, although some samples reduced at this temperature showed some indication of wustite.

Three possible explanations can be advanced for the slower reaction observed in the presence of argon:

(a) mass transfer limitations with argon present,
(b) blockage of reaction sites by adsorbed argon, and
(c) a lower sample temperature in the presence of argon.

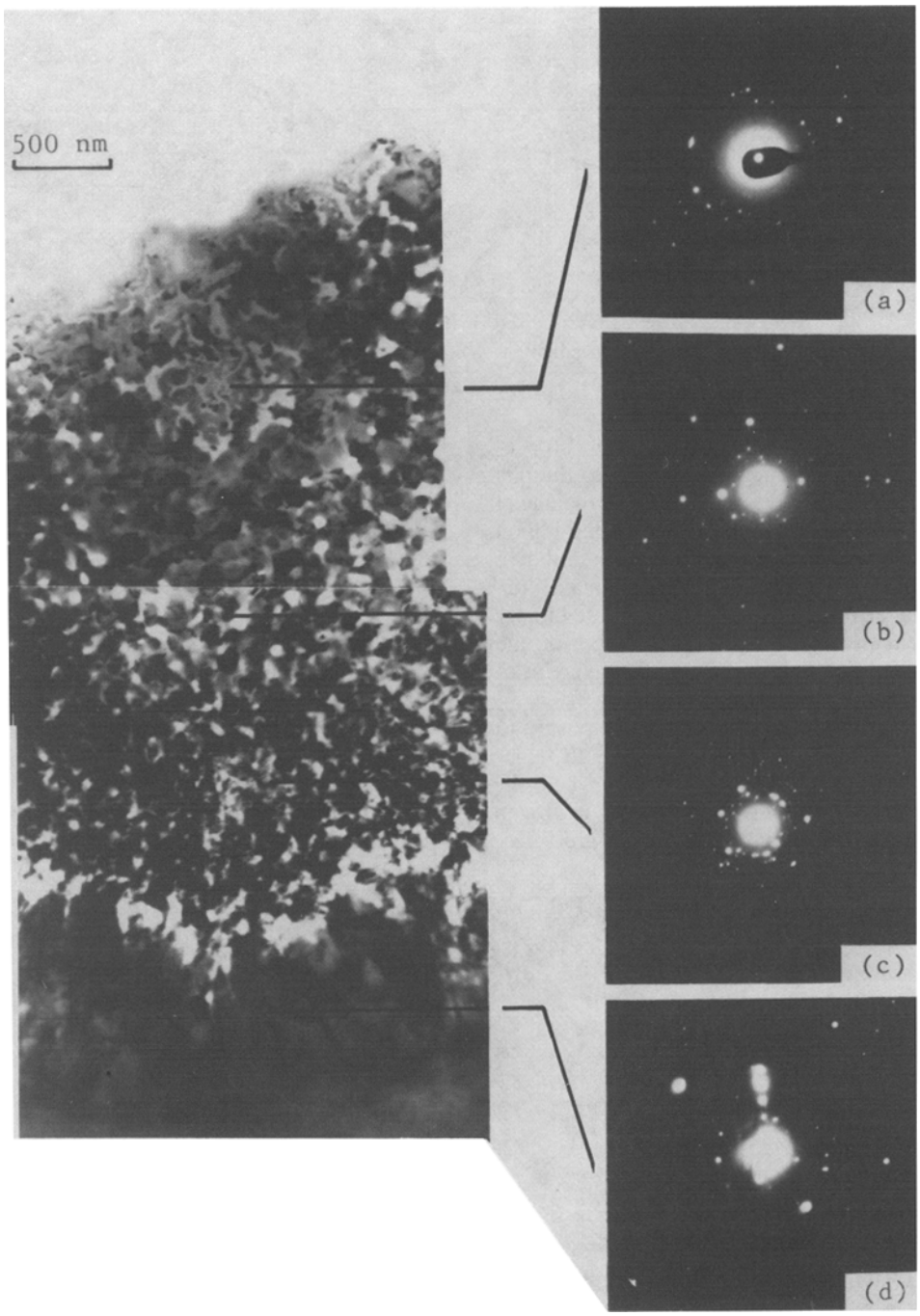

Fig. 4 — Selected area diffraction patterns from different reaction zones. Corresponding structures are porous iron (*a*), polycrystalline magnetite (*b*) and (*c*), and lath magnetite (*d*). The hematite specimen was reduced by 270 P pure H_2 at 387 °C for 14 min and 40 sec.

Estimation of a mass transfer coefficient is precluded by the complicated geometry of the cell and the microscopic nature of the sample. However, the diffusion coefficient for H_2-H_2O at 270 P total pressure, 387 °C is estimated to be 1.3×10^5 mm^2/s from the Fuller *et al.* correlation[39] while that for H_2-Ar at 5.3 kP, 610 °C is 10^4 mm^2/s. It seems likely that this order of magnitude difference in diffusion coefficient would result in a much lower mass transfer coefficient in the presence of argon. Explanation (b) appears unlikely since neither chemical nor physical adsorption of argon is expected under these experimental conditions. Finally, explanation (c) is made unlikely by the fact that the heat required to bring the flowing gas from room to reaction temperature is less than 2 pct of the heat generated electrically in the environmental cell for the case of argon present.

B. *Magnetite Reduction*

Figure 9 is a sequence of micrographs showing the reduction of magnetite by pure hydrogen (270 P) at 300 °C. Faceted pits appeared after approximately four minutes (see,

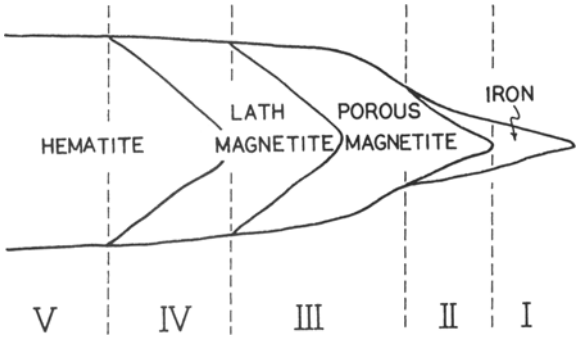

Fig. 5—Schematic diagram of the cross-section of the specimen illustrating five different zones corresponding to Fig. 4.

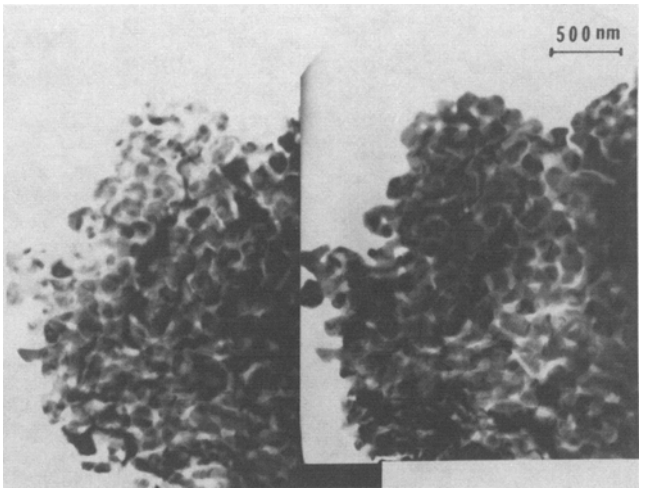

Fig. 7—Stereo pair of electron micrographs revealing the crystalline morphology of hematite after 8 min reduction under 5.3 kP of 10 pct H_2/90 pct Ar mixture at 610 °C. Note that no pores were developed.

for example, the left of the micrograph marked 306 seconds). Iron then nucleated in a region adjacent to the pits (left of center in micrograph at 375 seconds), and the nuclei then grew across the magnetite surface. This same region before and after 13 minutes exposure to hydrogen is shown in Figure 10 at lower magnification. Some of the nucleation sites are indicated by arrows and appear to be in the thinner regions of the specimen. Nucleation did not occur on the edge of the specimen which is in contrast to the behavior of hematite single crystal on reduction by hydrogen.

The faceted pits were observed to grow on exposure to hydrogen, starting with a triangular shape and then becoming six-sided. This can be seen in Figure 11 where the left micrograph depicts 16 minutes exposure to hydrogen and the right micrograph, 17 minutes. Selected area electron diffraction revealed that the region of the pits was still magnetite; Figure 12 shows the bright-field and dark-field images of a region containing a group of pits, and the parallelism of some pit edges (*e.g.*, the upper edges in this figure) should be noted. The pits are enveloped by the advancing reaction front, and if they are sufficiently large or deep then they affect the morphology of the iron formed from the pitted region.

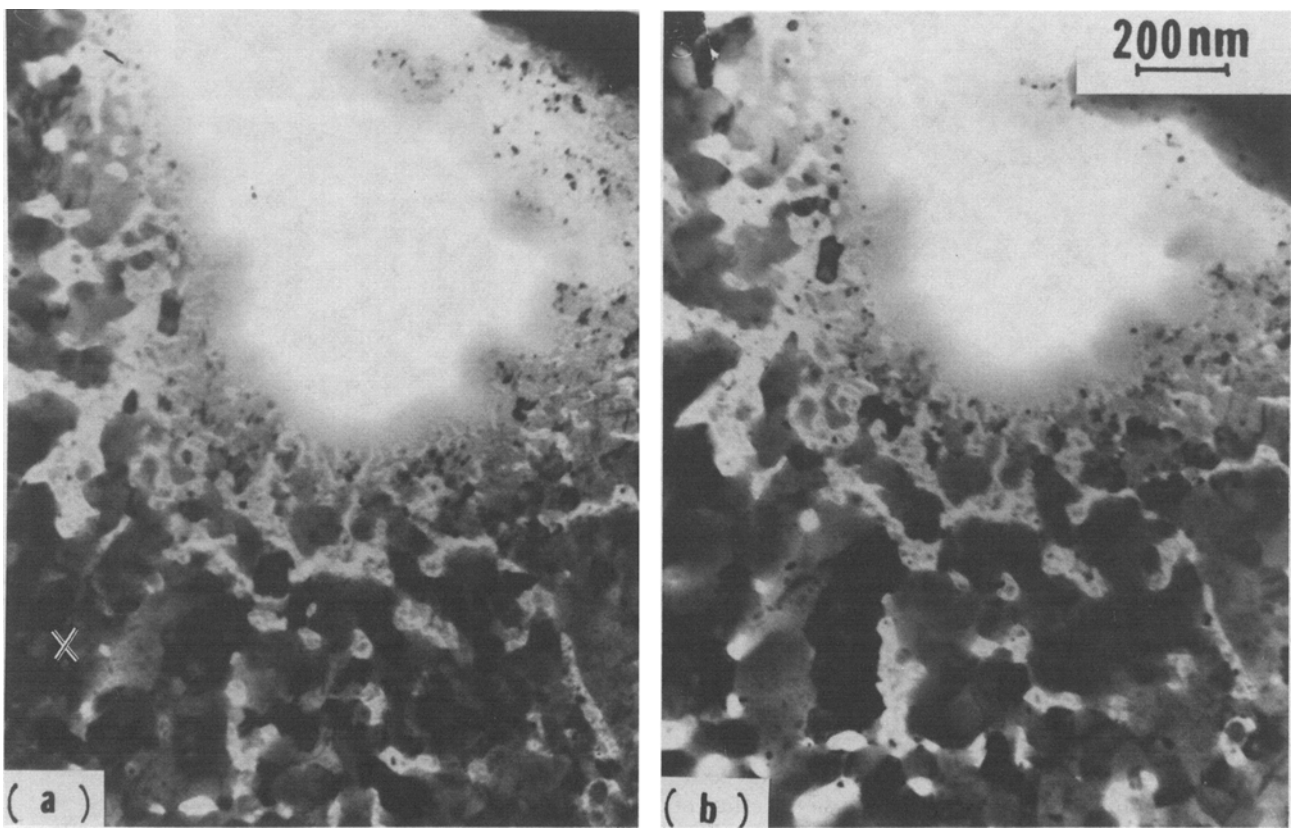

Fig. 6—Electron micrographs of porous iron obtained by reducing hematite with 270 P pure hydrogen at 417 °C for 3 min (*a*) and 14 min (*b*). Note that a large portion of the morphology is unchanged except the area near the marker 'X' where the retraction of the residual magnetite and the enlargement of pore size can be seen.

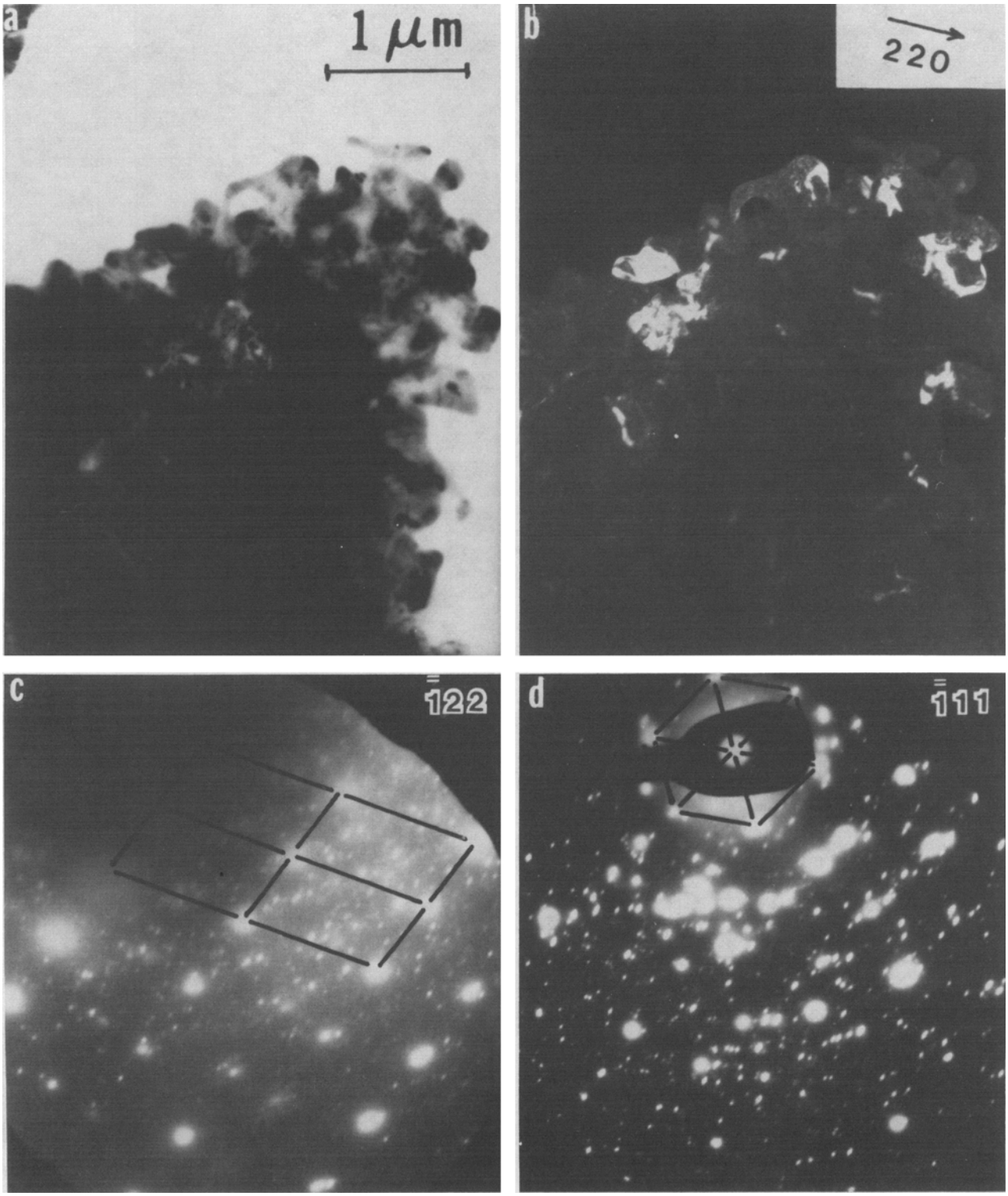

Fig. 8—Bright- (*a*) and dark- (*b*) field images of magnetite product after 10 min reduction time under the same conditions as above. Diffraction patterns (*c*) and (*d*), corresponding to [122] and [111] zone axes of magnetite single crystal patterns, were taken from the center and the tip of (a), respectively.

In the early stages of reduction the iron formed was oriented with respect to the host magnetite single crystal. This is seen in Figure 13 which is after 21 minutes exposure to 130 P of hydrogen at 330 °C. The diffraction pattern of α iron is a spot pattern rather than a ring pattern which would have occurred if non-oriented polycrystalline iron had been formed.

Figure 14 shows a region that has been partly reduced at 1.3 kP and 400 °C. (a) is the bright-field image, while (c) and (d) are the dark-field images taken from rings A and B in the diffraction pattern that correspond to iron and magnetite, respectively. The porous iron that is rapidly formed by this one-minute exposure at this higher temperature contains considerable residual magnetite, but this residual mag-

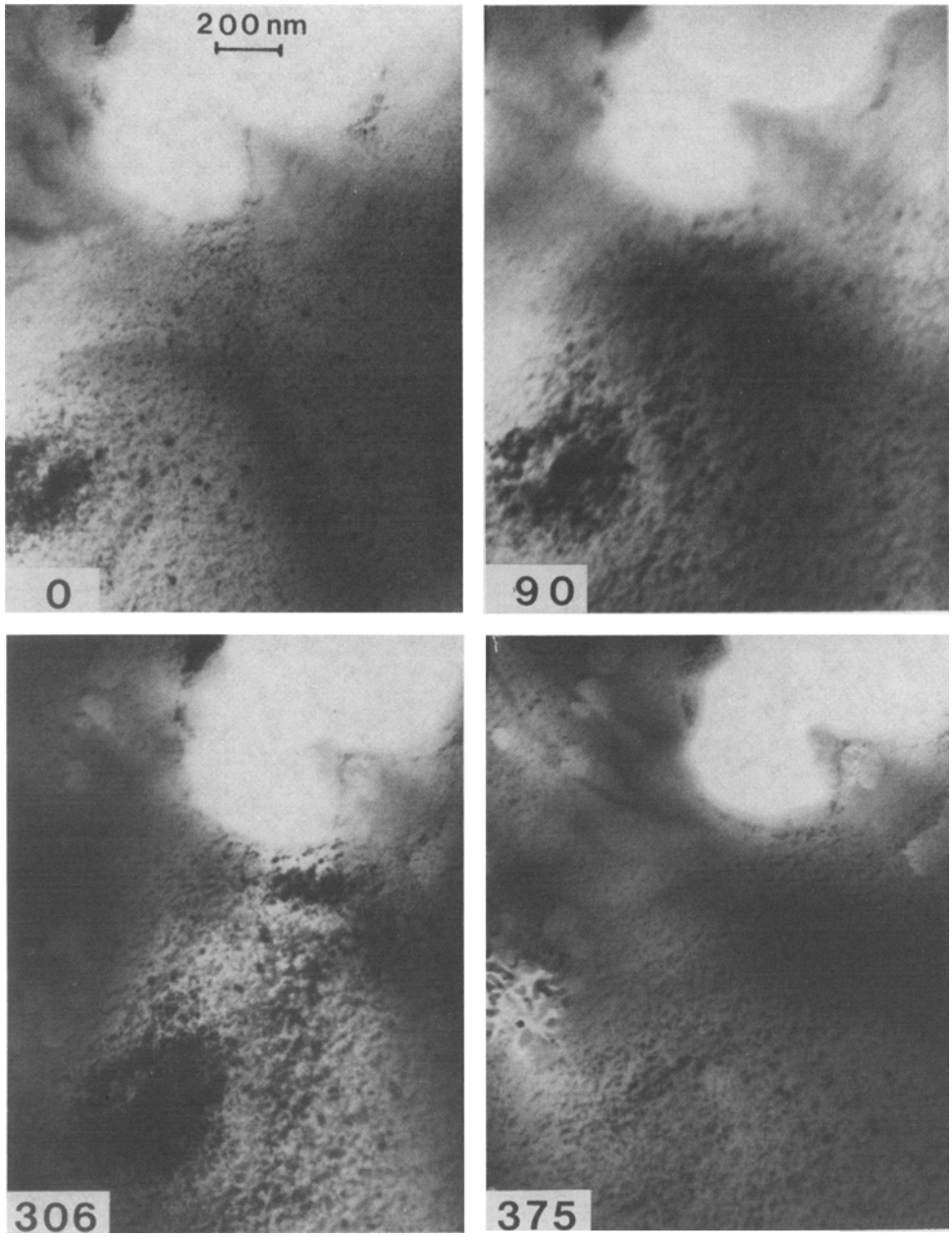

Fig. 9—Sequence electron micrographs showing the reduction of magnetite. The specimen was reduced by 270 P in pure hydrogen at 300 °C. Numbers inserted are the reduction time in seconds.

netite has become polycrystalline as reaction disrupts the original single crystal structure. The spotty rings appearing in the diffraction pattern are for α iron suggesting orientation of the iron in the early stages of reaction followed by disruption of this orientation as reaction proceeds.

Reduction temperature has a significant effect on the morphology of the iron formed, as reported by others.[11] This is seen in the results depicted in Figure 15. (a) shows the magnetite-iron interface after 10 seconds reduction with 2.7 kP of hydrogen at 350 °C. Note the small (10 to 50 nm) grains of iron that have been formed at this stage. (b) is the dark-field image. The sample was then brought to 500 °C in vacuum and held for 2 minutes (c), at which point the iron had pulled away from the magnetite producing the fissure running diagonally across the micrograph. (d) is the dark-field image. There had been much coarsening of the iron structure. The temperature was then lowered to 300 °C and the sample again exposed to hydrogen. Reaction started to the right of the fissure and proceeded slowly with the iron produced having a coarse structure. (e) shows the appearance 2 minutes after reexposure.

The shrinkage that resulted in the fissure of Figure 15 can occur even under conditions of uninterrupted reaction and the porous iron produced by reduction of magnetite was frequently observed to be fissured, sometimes in the star-shaped pattern reported by Pluschkell and Sarma;[40] see Figure 16. These large fissures in iron produced by reduction of single crystal magnetite were not found in the iron

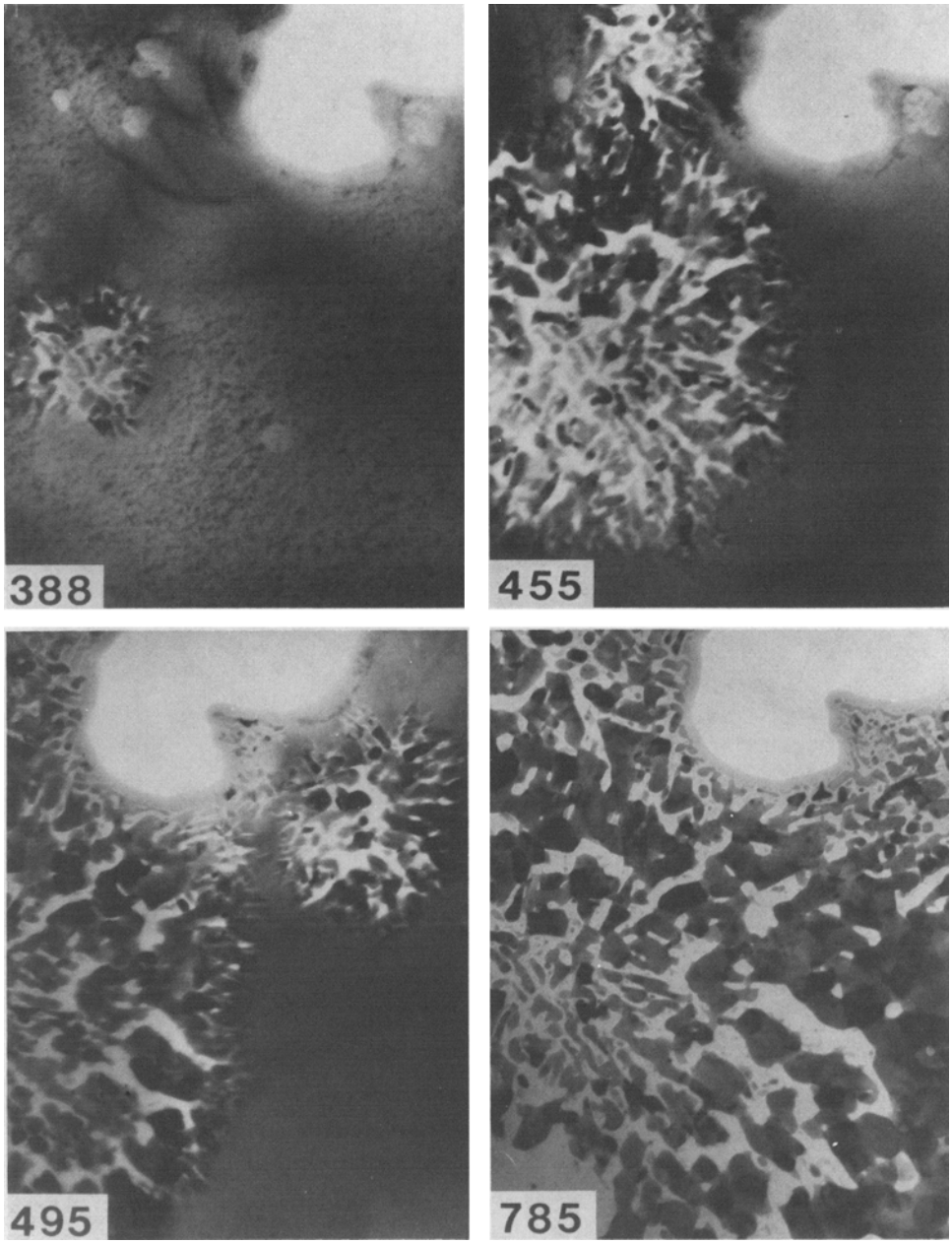

Fig. 9 Cont. — Sequence electron micrographs showing the reduction of magnetite. The specimen was reduced by 270 P in pure hydrogen at 300 °C. Numbers inserted are the reduction time in seconds.

produced by reduction of hematite. A possible explanation is as follows.

The reduction of hematite proceeds with the formation of small crystals of magnetite which are then reduced to iron. The volume change on reducing magnetite to iron can readily be accommodated by shrinkage of these grains, resulting in an iron of higher porosity than the parent magnetite but without fissures. In reducing single crystal magnetite, strains due to volume change develop over the whole width of the growing iron nucleus and eventually become sufficiently large to disrupt the nucleus, forming large fissures and changing the orientation of the nucleus to the parent lattice.

When magnetite specimens were contacted with hydrogen-argon mixtures, reaction proceeded very slowly (as in the case of hematite reduction). Figure 17 is a sequence of micrographs of a specimen exposed to 10 pct H_2/90 pct Ar at 350 °C and 1.3 kP total pressure. In this instance the time on the micrographs is in *minutes* and, in order to achieve significant reaction in the microscope time available, iron had been nucleated by prior exposure to pure hydrogen at 1.3 kP, 400 °C for 1 minute. The micrographs can be interpreted as showing a coarsening of the iron nucleus together with the formation of a hexagonal pit occupied by the iron phase. The walls of the pit appear to become smooth and vertical as time elapses; this is sketched in Figure 18.

Cracks and dislocation loops may play a role in the reduction. In Figure 19, which is of a specimen exposed to 10 pct H_2/90 pct Ar at 6.6 kP total pressure and 514 °C, a

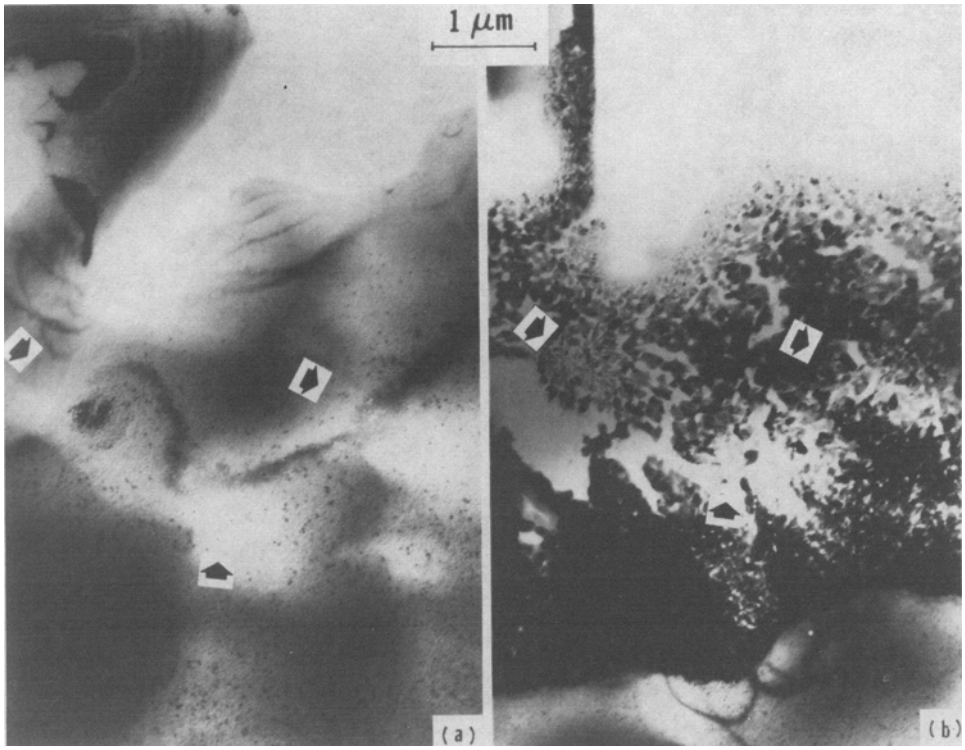

Fig. 10 — Overview of the region of Fig. 9 before (*a*) and after (*b*) 13 min reduction. The arrows indicate the thinner region of the specimen, which might be the favored sites for nucleation of the iron phase.

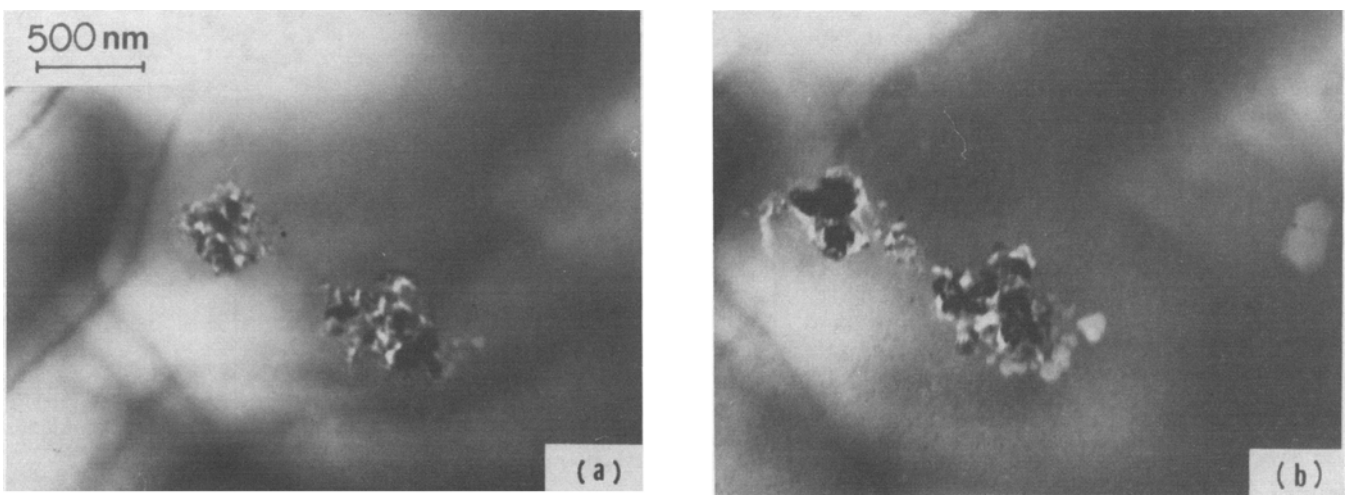

Fig. 11 — Electron micrographs showing the development of faceted pits on partially reduced magnetite. The specimen was brought back to room temperature after the first stage reduction by 270 P pure hydrogen at 300 °C for 14 min, then was reduced again at the same temperature for 2 (*a*) and 3 (*b*) min.

crack runs horizontally across the middle of the sample. Pits have formed at this crack during reduction and elongated in a direction perpendicular to the crack. The pits appear to grow along dislocation loops (*e.g.*, to the right of the figure).

C. *Wustite Reduction*

Even though final thinning of the specimens was under vacuum, samples of wustite were found to contain small magnetite colonies. Electron diffraction showed the colonies (approximately 1 μm across) to be epitaxial with the host wustite. Wustite is thermodynamically unstable below 570 °C and may be expected to disproportionate to iron and magnetite below that temperature. However, the rate of disproportionation is slow so that wustite can be regarded as metastable. Preliminary studies were carried out in vacuum to follow the expected thermal decomposition of the wustite to magnetite and iron. Figure 20 is a sequence of micrographs taken at 500 °C; the indicated time is in minutes. The black particles on the specimen are contamination and appear to be inert. Some slight changes are observable (upper

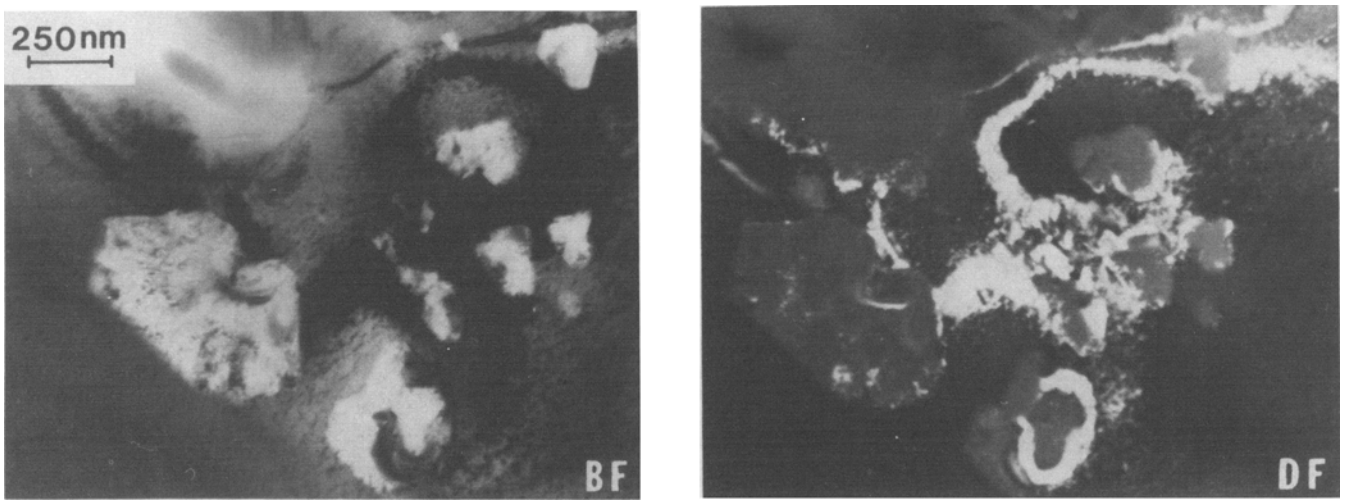

Fig. 12—Bright- and dark-field images of faceted pits showing a close relationship between the pits and the parent magnetite matrix.

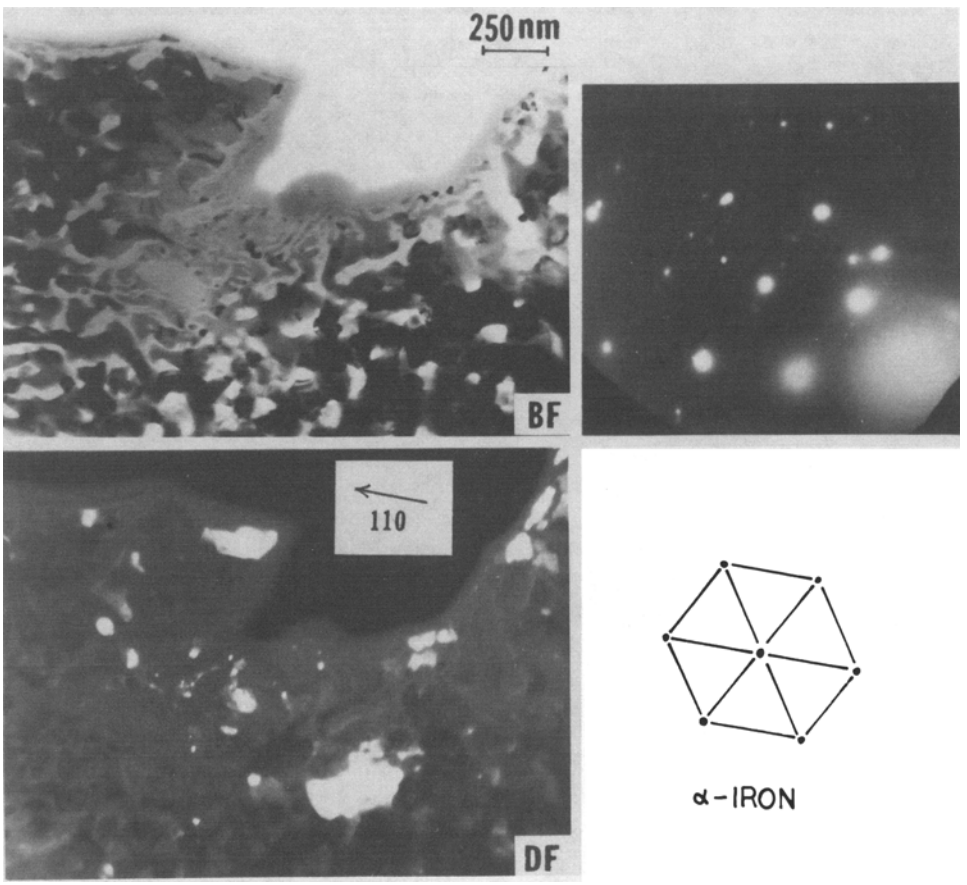

Fig. 13—Bright- and dark-field images of the magnetite specimen after reduction with 130 P hydrogen at 330 °C for 21 min.

right) after a few minutes, but even after 18 minutes the changes to the specimen are not large. The triangular area to the left is a growing magnetite platelet (identified by electron diffraction); presumably iron produced by the decomposition is incorporated in the host wustite by the stoichiometry range of that compound or is disseminated as areas too small to be visible. Figure 21 is a micrograph of the same area of wustite after 40 minutes at 500 °C in vacuum. The minute rectangular areas are too small for identification by selected area diffraction but may be iron. When the sample was brought to 600 °C, the magnetite and rectangular areas were observed to disappear slowly (Figure 21(c)).

The reduction of wustite by hydrogen yields iron of a structure comparable to that from magnetite reduction. Figure 22 is a sequence of micrographs of a sample exposed

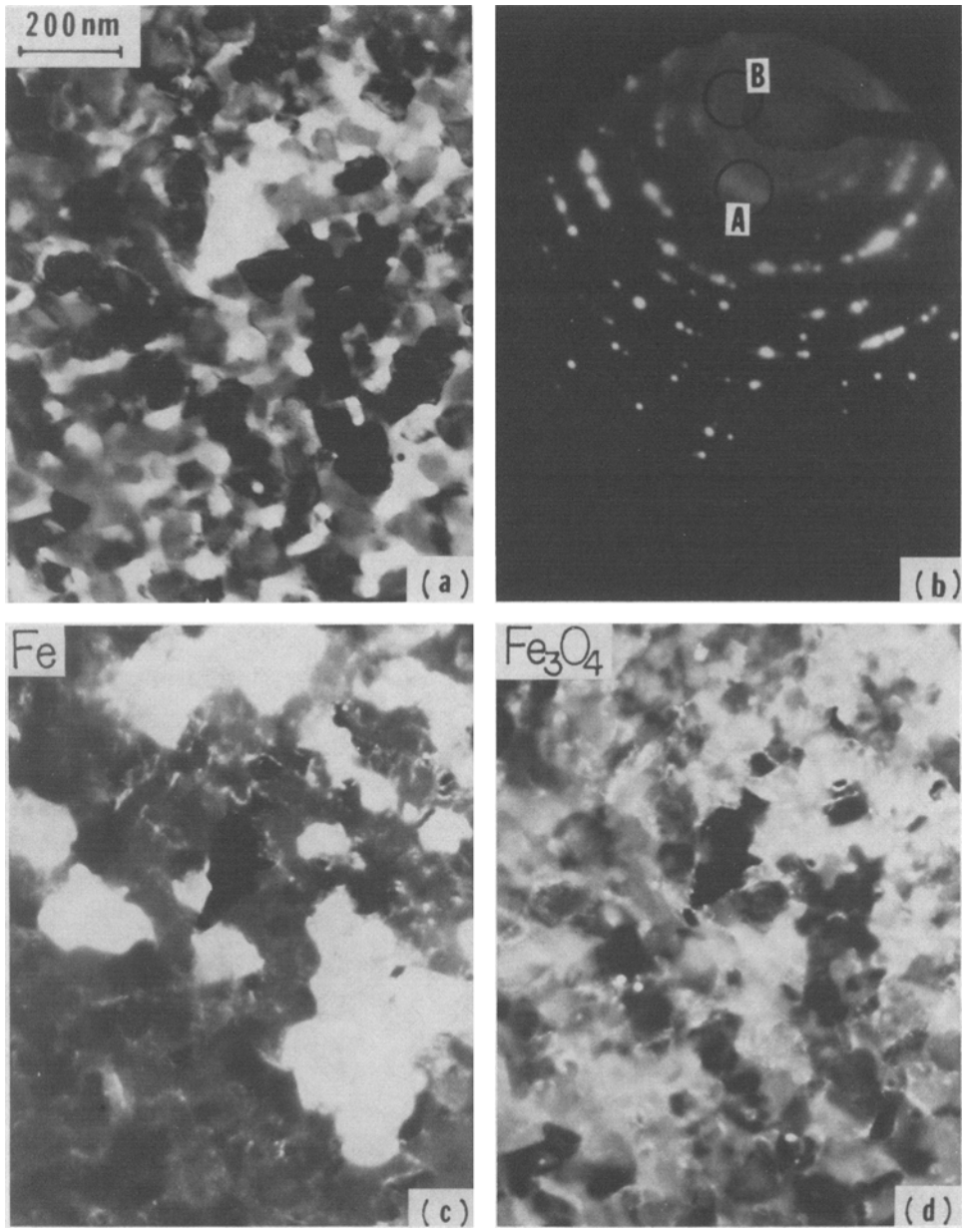

Fig. 14—(*a*) Bright-field image of porous iron formed in reducing magnetite with 1.3 kP pure hydrogen at 400 °C for 1 min. (*c*) and (*d*) are corresponding dark-field images from A and B reflections indicated in the electron diffraction pattern (*b*). (c) reveals iron clusters and (d) reveals residual magnetite.

to 1.3 kP of hydrogen at 355 °C. Three magnetite clusters appear in the center of the micrograph of the original wustite and they were centers for nucleation of the iron, along with the edge of the specimen. The rapidity of the reduction reaction, compared to the disproportionation seen in Figure 14, should be noted. Neither an incubation period nor faceted pits were observed. Coarsening of the pores as reaction proceeds should be noted. Selected area diffraction patterns (Figure 23) from the center of the micrograph after 2 minutes reaction showed the presence of both polycrystalline iron and magnetite. The occurrence of magnetite* in the diffraction pattern at first appears paradoxical and leads to the suggestion that reduction is being accompanied by disproportionation, the latter being promoted by the former (perhaps by the iron produced by reduction). However, if iron produced by reduction promotes disproportionation, then its effect must be highly localized. This is evident from an experiment in which reduction was halted after 2 minutes followed by holding the wustite sample at 400 °C in vacuum for 10 minutes. No clear evidence of disproportionation could be seen during this ten minutes.

At lower pressures of reducing gas and higher temperatures, disproportionation becomes more evident. Figure 24 is a set of micrographs of a sample reduced using 66 P of hydrogen at 450 °C. The advancing iron phase due to reduction can be seen sweeping through the specimen from the upper left in the micrograph at 485 seconds. Stereomicrographs reveal that the near rectangular structures evi-

*It is likely that this magnetite is not that present in the initial wustite; that magnetite is epitaxial, while the magnetite in Figure 17 yields a strong ring pattern.

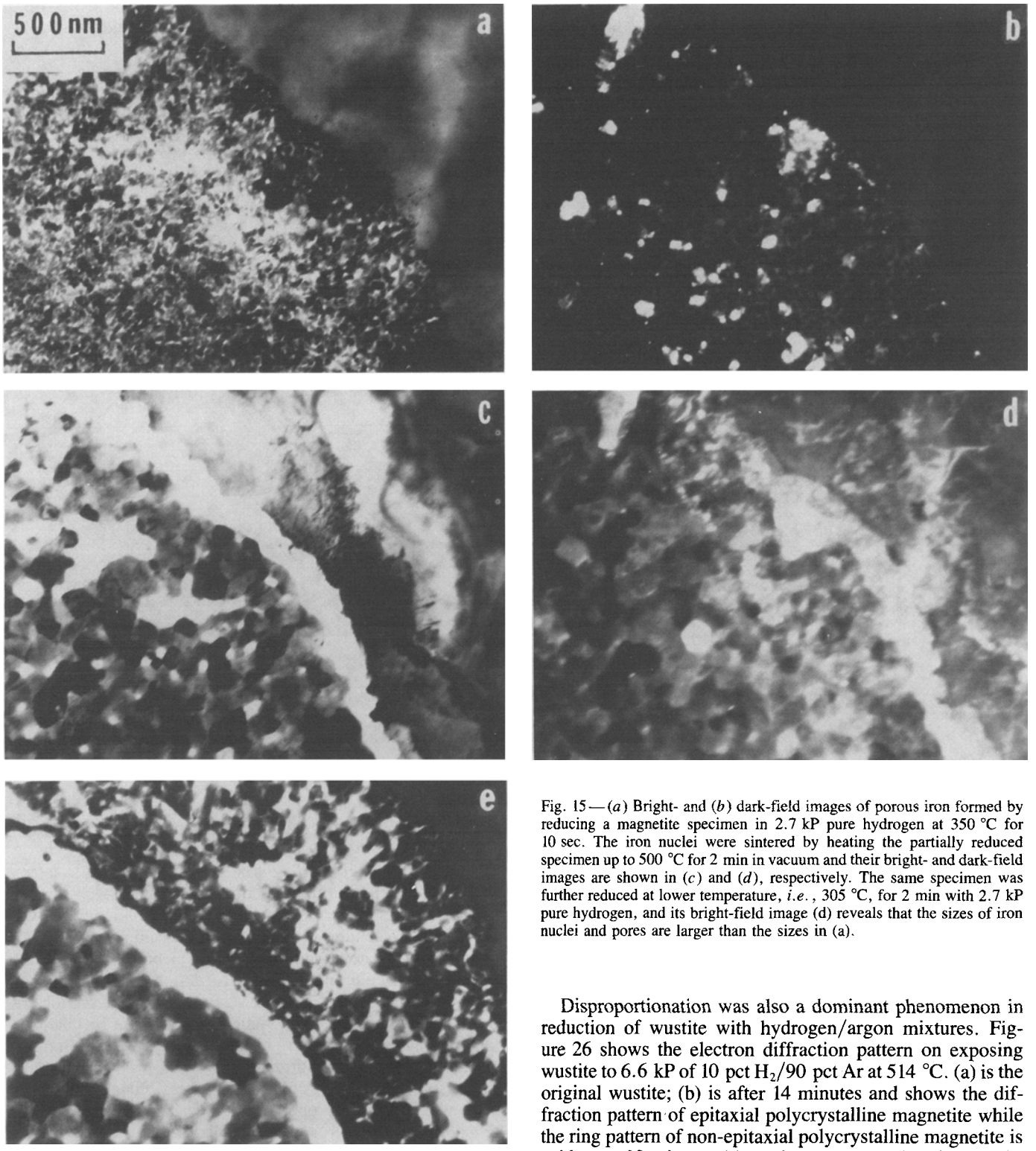

Fig. 15—(*a*) Bright- and (*b*) dark-field images of porous iron formed by reducing a magnetite specimen in 2.7 kP pure hydrogen at 350 °C for 10 sec. The iron nuclei were sintered by heating the partially reduced specimen up to 500 °C for 2 min in vacuum and their bright- and dark-field images are shown in (*c*) and (*d*), respectively. The same specimen was further reduced at lower temperature, *i.e.*, 305 °C, for 2 min with 2.7 kP pure hydrogen, and its bright-field image (d) reveals that the sizes of iron nuclei and pores are larger than the sizes in (a).

dent in the upper two micrographs are pits bounded by raised areas (darker regions). A possible explanation in terms of disproportionation is provided in Figure 25 where the Fe_3O_4 phase (being more voluminous than FeO) protrudes above the FeO surface while the less voluminous Fe phase sinks below it.

Disproportionation was also a dominant phenomenon in reduction of wustite with hydrogen/argon mixtures. Figure 26 shows the electron diffraction pattern on exposing wustite to 6.6 kP of 10 pct H_2/90 pct Ar at 514 °C. (a) is the original wustite; (b) is after 14 minutes and shows the diffraction pattern of epitaxial polycrystalline magnetite while the ring pattern of non-epitaxial polycrystalline magnetite is evident at 30 minutes (c), and stronger at 160 minutes (d). Iron does not appear in these diffraction patterns because no iron was within the region covered by the aperture used.

The appearance of iron produced by reduction using this gas mixture (at 6.6 kP, 373 °C, 47 minutes) is seen in Figure 27 together with the diffraction pattern identifying iron. The faceted nature of this structure should be noted; many edges are parallel to the direction indicated by the arrow.

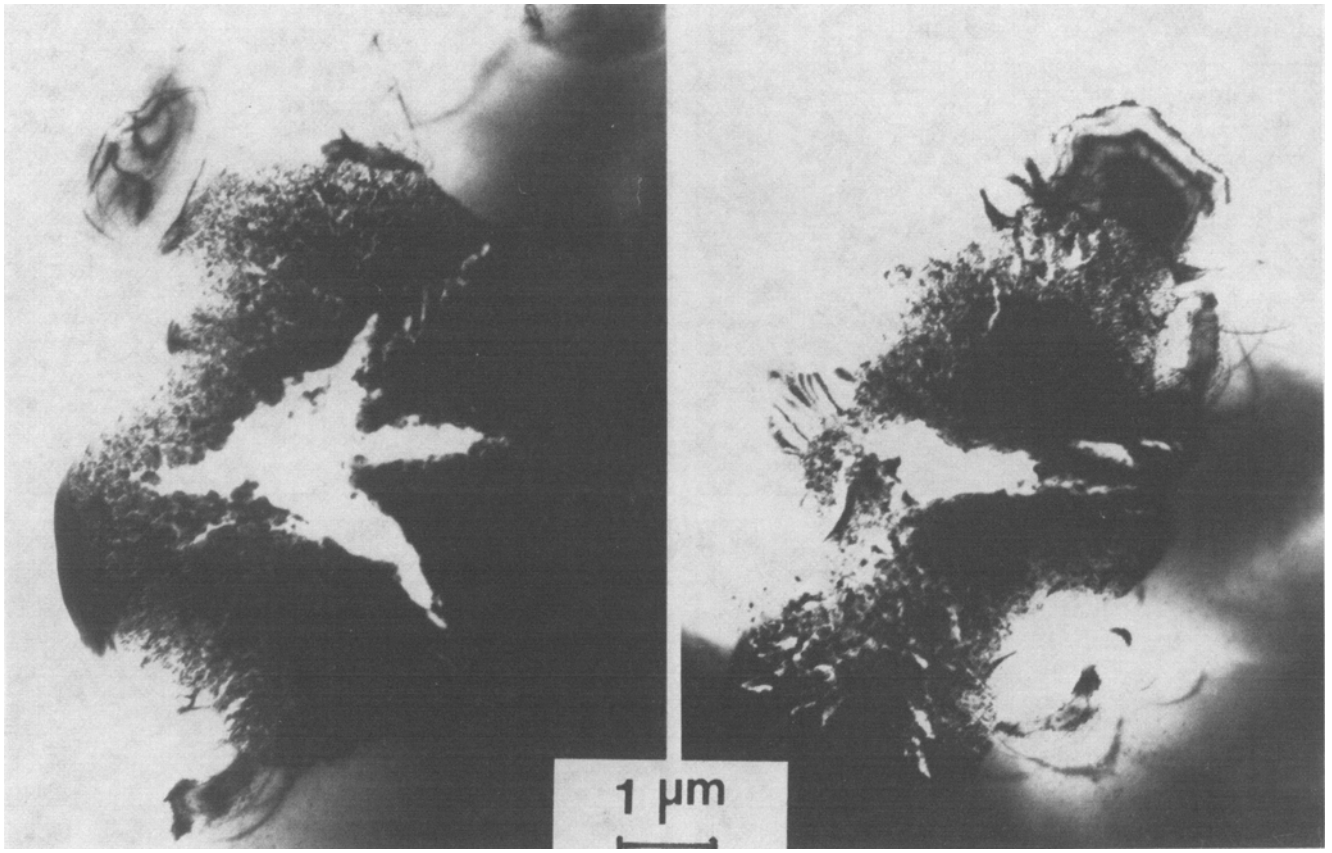

(*a*) (*b*)

Fig. 16—(*a*) Typical star-shaped pores in product iron. (*b*) Pores formed in one iron cluster only when two iron nuclei coalesced. The magnetite specimen was reduced by 270 P hydrogen at 300 °C for 13 min and 5 sec.

IV. CONCLUSIONS

In situ studies of hematite reduction have been carried out using hydrogen and using a hydrogen/argon mixture. Reduction by hydrogen was faster and started from nucleation sites on the edge of the sample. Four clearly distinguishable zones were revealed: unreacted single crystal hematite which usually forms lath magnetite under the conditions of the study, the lath magnetite which rapidly transforms to porous magnetite, porous magnetite, and porous iron. The rate controlling step appears to be the reduction of magnetite to iron. Reduction with the hydrogen/argon mixture proceeded much more slowly and across the whole surface, producing granular magnetite. Most of the observations are consistent with those of prior *ex situ* investigations.

On reducing magnetite with pure hydrogen, under the conditions of this investigation, incubation periods were observed. During these incubation periods no iron was evident, but faceted pits formed and grew on the magnetite surface. Nucleation of iron typically occurred near these pits which were then engulfed by the advancing porous iron phase. Iron formed in the early stages of reduction was epitaxial with the host magnetite, but this orientation was disrupted as reaction continued. Reduction temperature has an effect on the morphology of the iron produced, and fissures were found within the iron in many instances. When using pure hydrogen, the porous iron nuclei grew isotropically. With hydrogen/argon gas mixtures, reduction proceeded much more slowly. In the early stages of reduction faceted pits containing iron were formed while later these pits appeared to extend along dislocations.

Wustite was found to undergo slow changes when exposed under vacuum to the temperatures employed in this investigation. The change is thought to be disproportionation to magnetite and iron. On reduction with hydrogen, iron was formed with a morphology similar to that produced by hydrogen reduction of magnetite; neither an incubation period nor faceted pits were observed. Polycrystalline magnetite was found after some reaction, and it is conjectured that disproportionation both accompanies reduction and is promoted by it. Disproportionation was more evident on reduction using hydrogen/argon mixtures; as in the case of hematite and magnetite, reduction with this gas mixture was remarkably slow and (as in the case of magnetite) anisotropic.

This paper has employed an infrequently used experimental technique to examine microstructural aspects of the reduction of iron oxides by hydrogen. The investigation has been a restricted one, examining only single crystals at moderate temperatures and with little variation in gas pressure/composition. Nevertheless, the results to date sug-

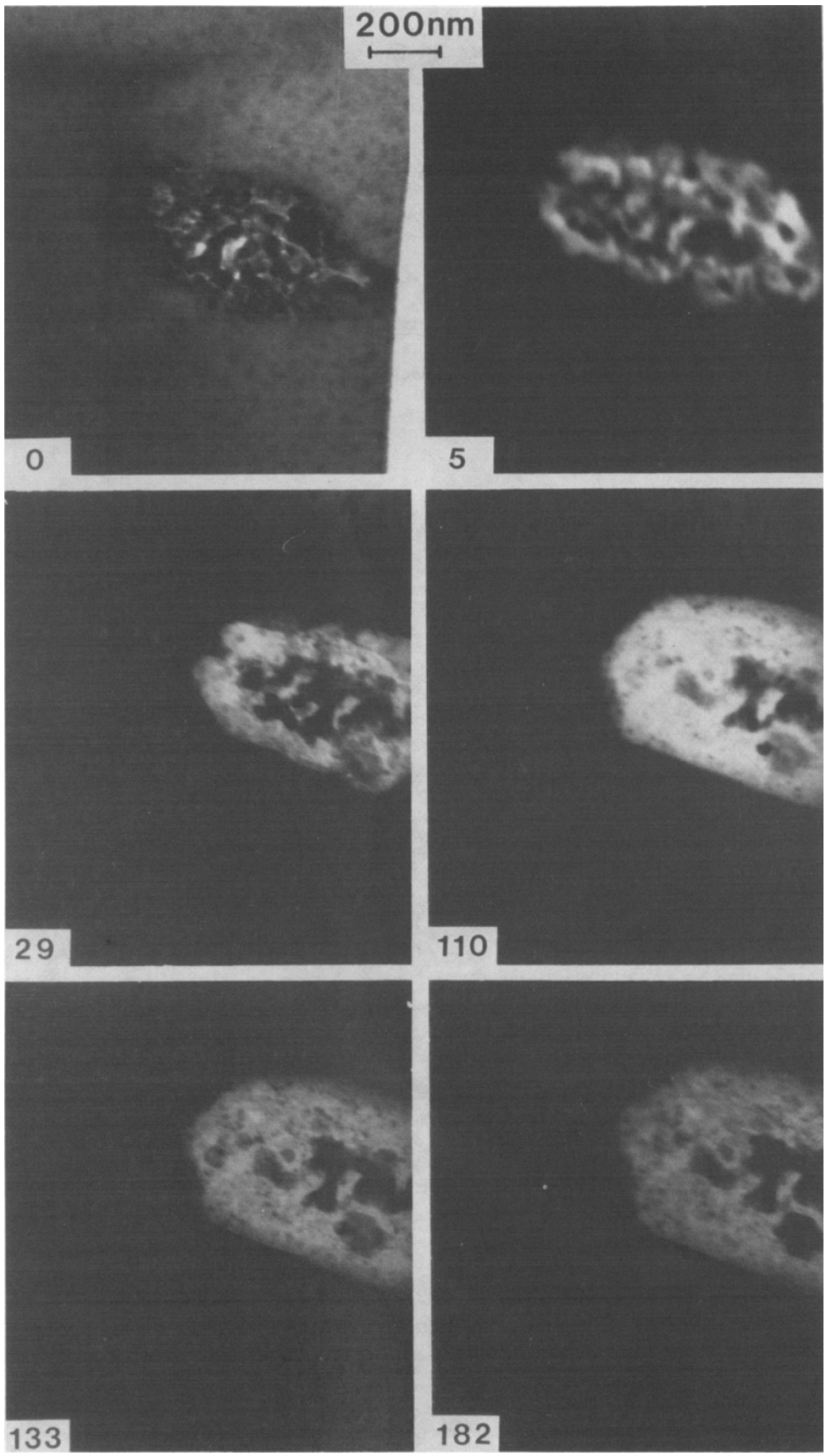

Fig. 17—Reduction occurs in several preferential directions with a low reducing potential gas mixtures, 10 pct H_2/90 pct Ar. The morphology shown in $t = 0$ is an iron cluster which was obtained by prior reduction in a pure hydrogen atmosphere. The partially reduced magnetite then was exposed to 1.3 kP 10 pct H_2/90 pct Ar at 350 °C. The morphology of the iron cluster changes during reaction. The number inserted is the time in minutes.

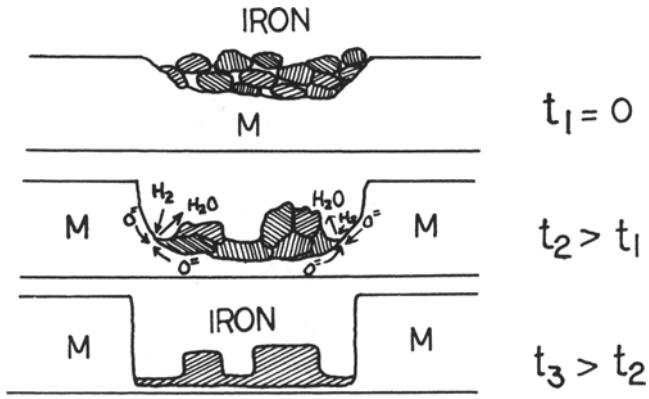

Fig. 18 — Schematic diagram illustrating the development of an iron cluster under low reducing potential.

Fig. 19 — A crack provides the reaction site for reduction under low reducing potential. The magnetite specimen was reduced at 514 °C using 6.6 kP 10 pct H_2/90 pct Ar. The numbers inserted are the reducing time in minutes.

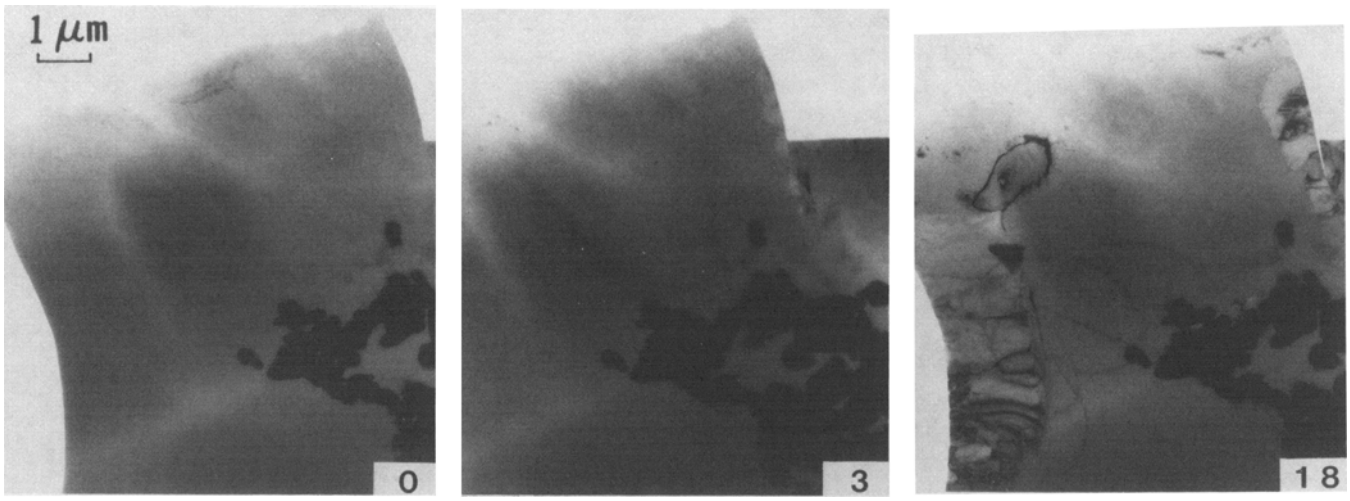

Fig. 20 — Disproportionation of wustite at 500 °C in vacuum. The numbers inserted are the duration time in minutes.

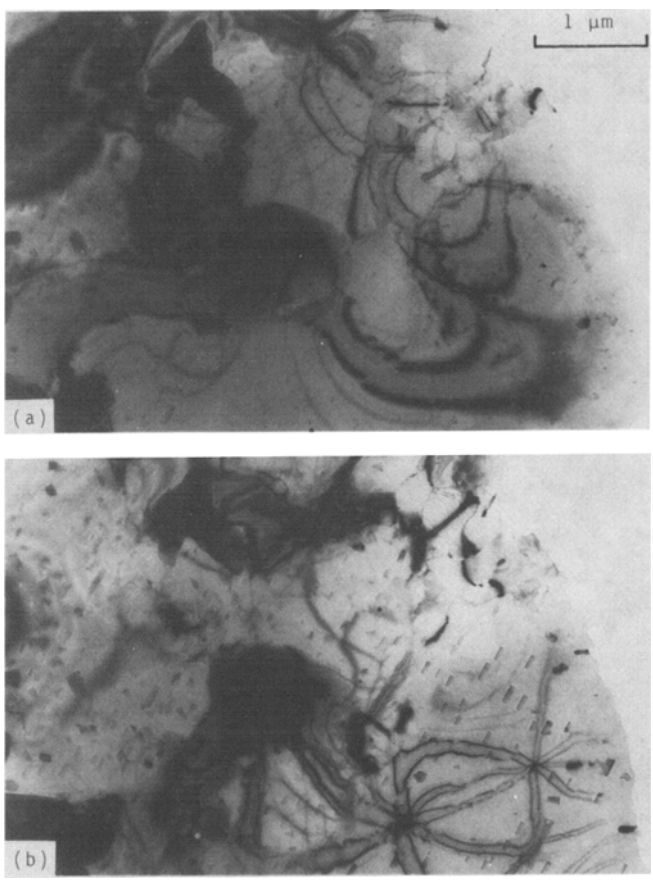

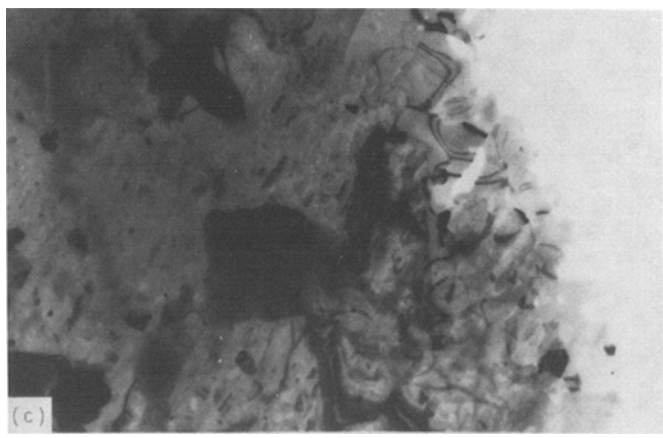

Fig. 21 — (*a*) Rectangular magnetite nuclei occurred after heating the wustite in vacuum at 500 °C for 40 min. (*b*) The magnetite nuclei grew preferentially in one direction. The electron micrograph was taken after 56 min. (*c*) The magnetite nuclei were dissolving back into the matrix after the temperature was brought up to 600 °C for 36 min.

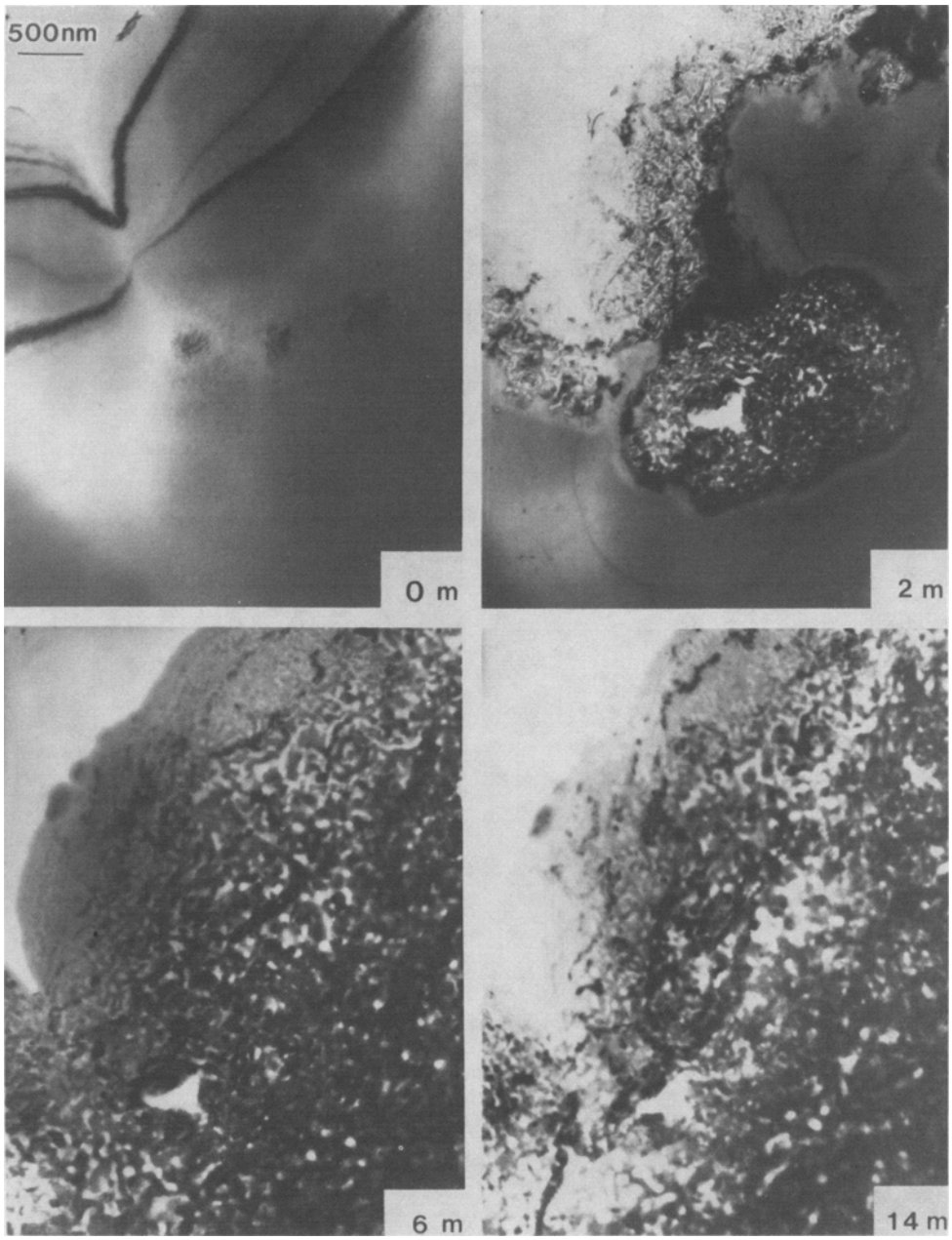

Fig. 22 — Sequence electron micrographs showing the reduction of wustite using 1.3 kP pure hydrogen at 350 °C for the time inserted in minutes. Morphological change is similar to that of magnetite reduction; however, there is no incubation period or faceted surface observed.

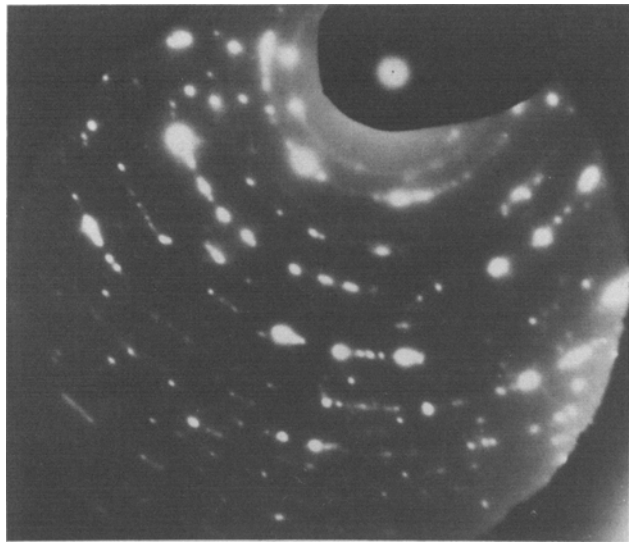

Fig. 23 — Typical diffraction pattern taken from iron nuclei showing that only iron and magnetite coexist.

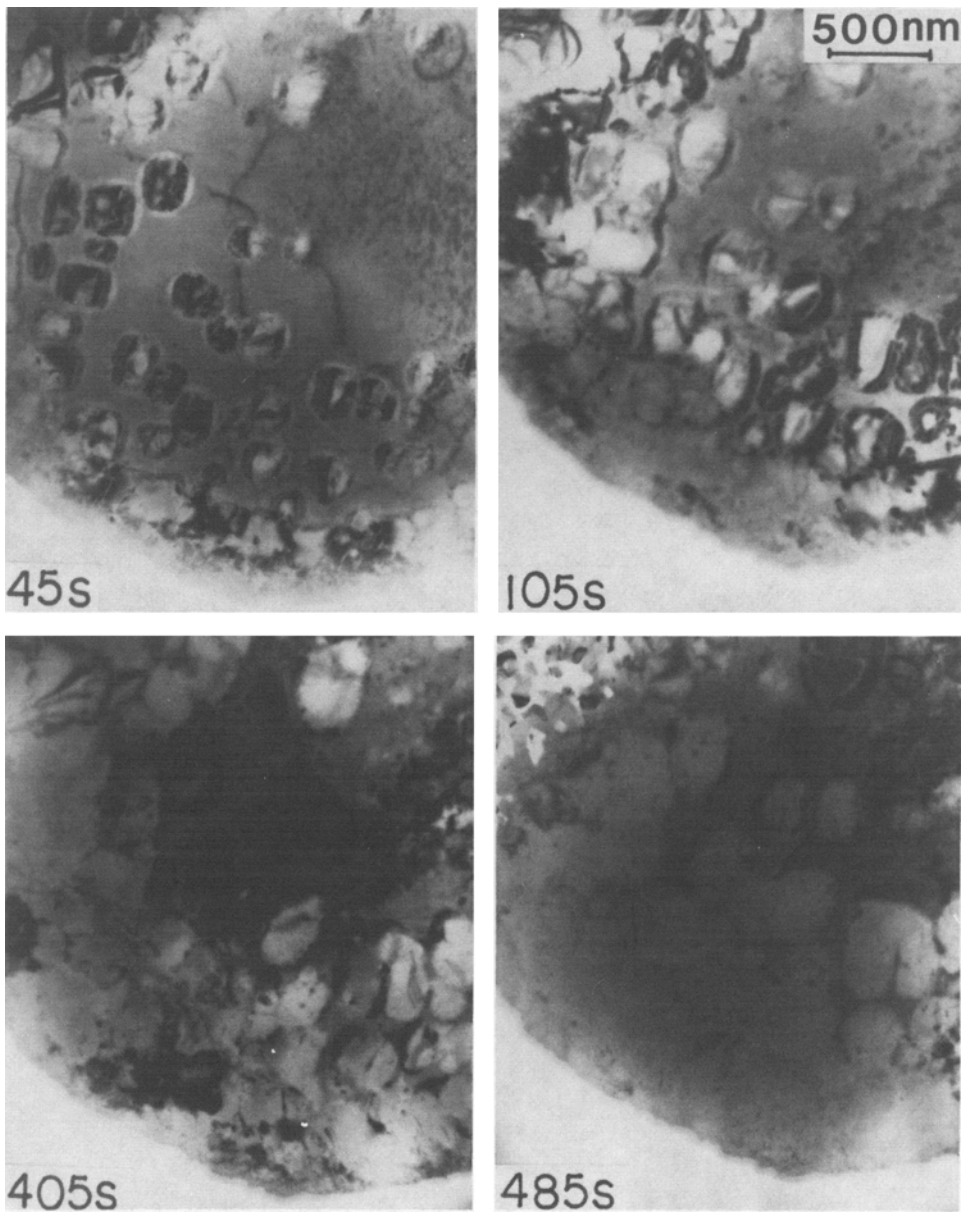

Fig. 24 — Electron micrographs of wustite reduction at 450 °C and 66 P of hydrogen. Disproportionation and reduction occurred simultaneously.

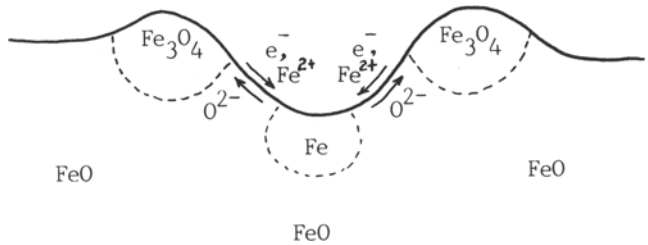

Fig. 25—Schematic illustrating the formation of a pit. Oxygen moves outward to build a wall of magnetite rich region and iron is left behind in the center of the pit.

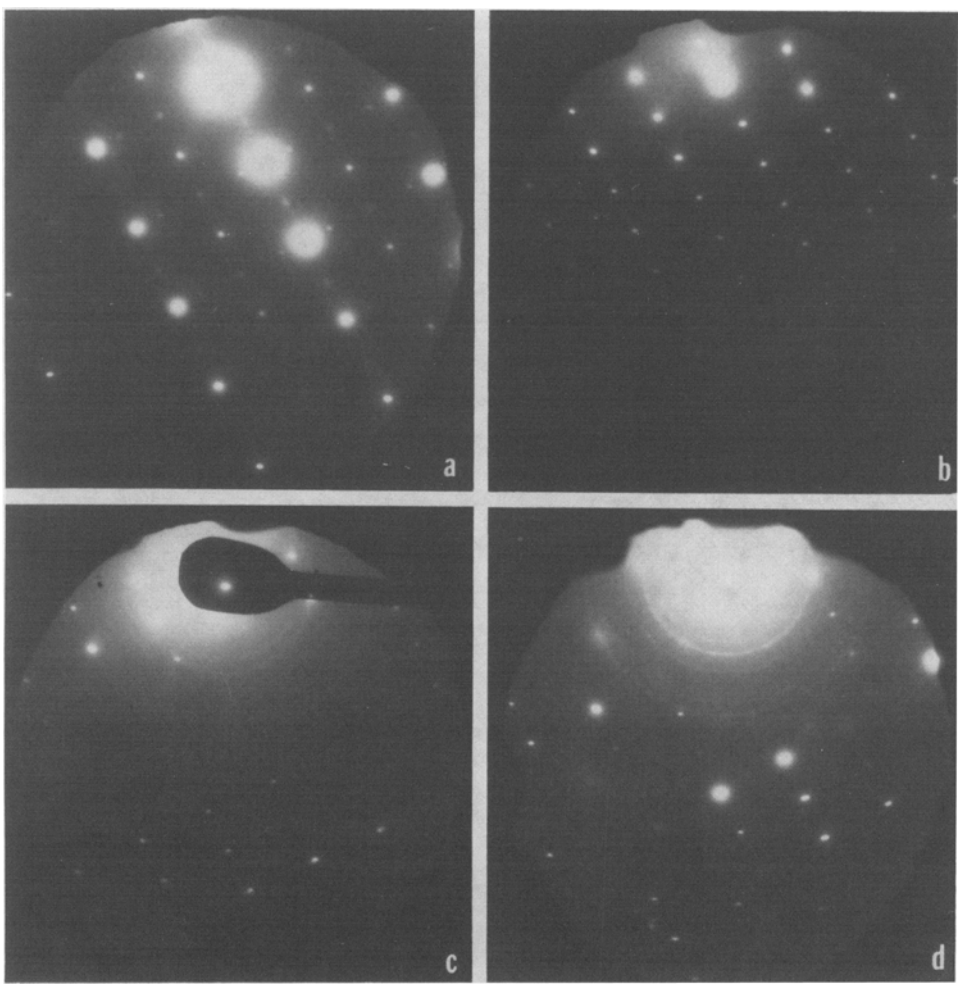

Fig. 26—Electron diffraction patterns showing the transformation of single crystal wustite → epitaxial crystal magnetite → polycrystalline magnetite. The specimen was reduced using 6.6 kP 10 pct H_2/90 pct Ar at 514 °C for 0 (*a*), 14 (*b*), 30 (*c*), and 160 (*d*) min, respectively.

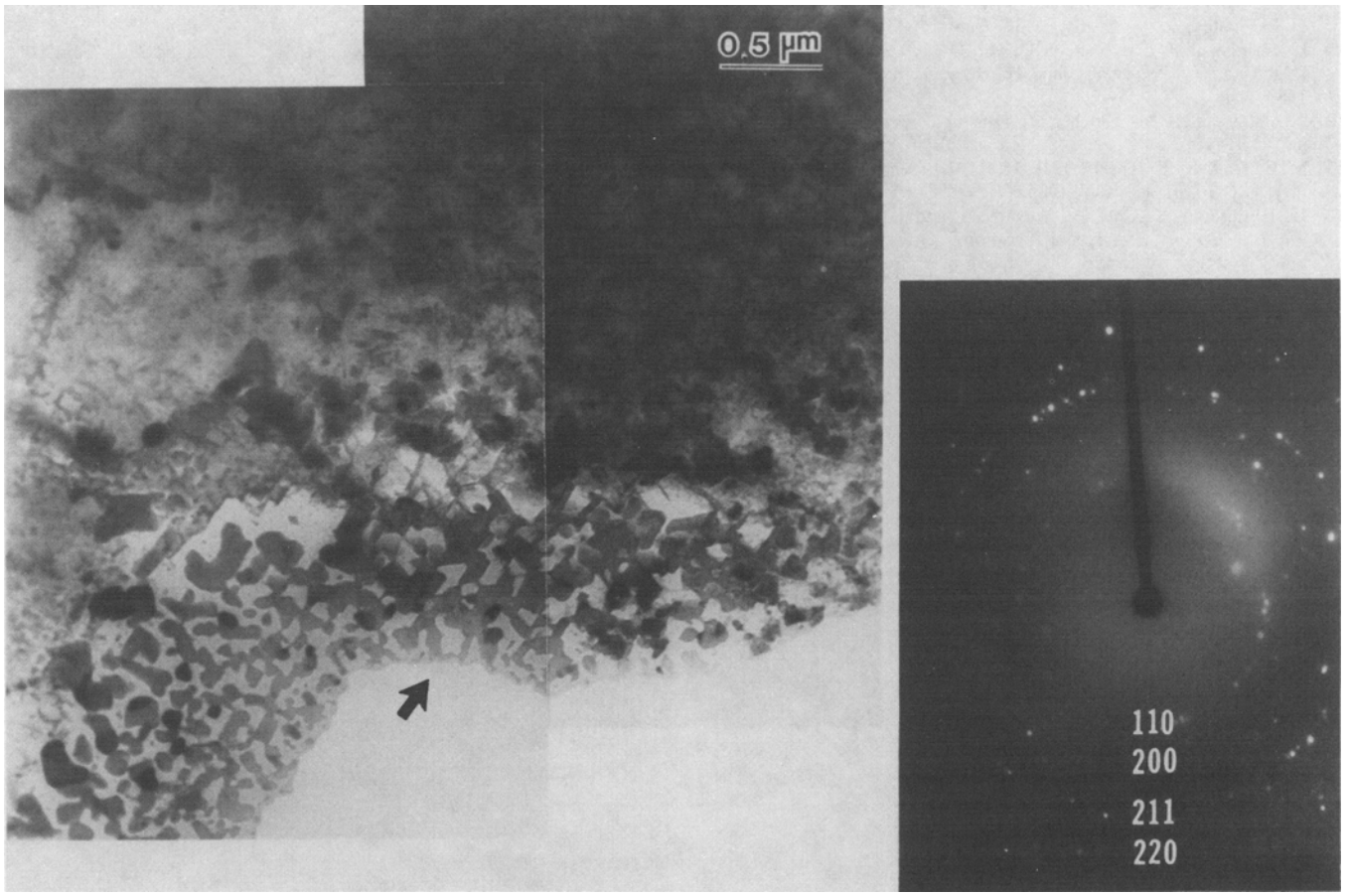

Fig. 27—Porous iron formed in a wustite specimen after reducing at 373 °C for 105 min using 5 pct H_2/95 pct Ar.

gest that the technique is a powerful one that can add to our understanding of this technologically important group of reactions.

ACKNOWLEDGMENT

This work was supported by the Director, Office of Energy Research, Office of Basic Energy Sciences, Materials Sciences Division of the United States Department of Energy under Contract Number DE-AC03-76SF00098.

REFERENCES

1. L. von Bogdandy and H. J. Engell: *The Reduction of Iron Ores*, Springer-Verlag, Berlin, 1971.
2. J. W. Evans and C. H. Koo: in *Rate Processes of Extractive Metallurgy*, H. Y. Sohn and M. E. Wadsworth, eds., Plenum Press, New York, NY, 1979, pp. 286-302.
3. J. Szekely, J. W. Evans, and H. Y. Sohn: *Gas-Solid Reactions*, Academic Press, New York, NY, 1976, pp. 339-47.
4. E. T. Turkdogan and J. V. Vinters: *Metall. Trans.*, 1971, vol. 2, pp. 3175-88.
5. S. K. El-Rahaiby and Y. K. Rao: *Metall. Trans. B*, 1979, vol. 10B, pp. 257-69.
6. Y. K. Rao and M. Moinpour: *Metall. Trans. B*, 1983, vol. 14B, pp. 711-23.
7. M. M. Al-Kahtany and Y. K. Rao: *Ironmaking and Steelmaking*, 1980, vol. 7, pp. 49-58.
8. S. K. El-Rahaiby and Y. K. Rao: *Trans. ISIJ*, 1980, vol. 20, pp. 287-91.
9. E. T. Turkdogan and J. V. Vinters: *Metall. Trans.*, 1972, vol. 3, pp. 1561-74.
10. J. W. Evans and K. Haase: *High Temp. Sci.*, 1976, vol. 8, pp. 167-77.
11. E. T. Turkdogan, R. G. Olsson, and J. V. Vinters: *Metall. Trans.*, 1971, vol. 2, pp. 3189-96.
12. C. H. Koo and J. W. Evans: *Trans. ISIJ*, 1980, vol. 19, pp. 95-101.
13. J. O. Edstrom: *J. Iron & Steel Inst.*, 1953, vol. 175, pp. 289-304.
14. J. O. Edstrom and G. Bitsianes: *AIME Trans.*, 1955, vol. 203, pp. 760-65.
15. H. Brill-Edwards, B. L. Daniell, and R. L. Samuel: *J. Iron & Steel Inst.*, 1965, vol. 203, pp. 361-68.
16. W. Pluschkell and H. Yoshikoshi: *Arch. Eisenhüttenw.*, 1970, vol. 41, pp. 715-21.
17. Y. K. Rao: *Metall. Trans. B*, 1979, vol. 10B, pp. 243-55.
18. A. V. Bradshaw and A. G. Matyas: *Metall. Trans. B*, 1976, vol. 7B, pp. 81-87.
19. D. H. St. John and P. C. Hayes: *Metall. Trans. B*, 1982, vol. 13B, pp. 117-24.
20. M. Moukassi, P. Steinmetz, B. Dupre, and C. Gleitzer: *Metall. Trans. B*, 1983, vol. 14B, pp. 125-32.
21. P. C. Hayes and P. Grieveson: *Metall. Trans. B*, 1981, vol. 12B, pp. 579-87.
22. A. Unal and A. V. Bradshaw: *Metall. Trans. B*, 1981, vol. 14B, pp. 743-52.
23. P. R. Swann and N. J. Tighe: *Metall. Trans. B*, 1977, vol. 8B, pp. 479-87.
24. J. R. Porter and P. R. Swann: *Ironmaking & Steelmaking*, 1977, vol. 5, pp. 300-07.
25. P. Baguley, D. H. St. John, and P. C. Hayes: *Metall. Trans. B*, 1983, vol. 14B, pp. 513-14.
26. J. A. Little, M. I. Perez, and J. W. Evans: Lawrence Berkeley Lab Report no. LBL-11473, 1980.
27. U. Finnstrom: *Scand. J. Metall.*, 1976, vol. 5, pp. 134-36.
28. R. A. Rapp: *Metall. Trans. A*, 1984, vol. 15A, pp. 765-82.

29. R. T. K. Baker and P. S. Harris: *J. Phys. E.*, 1972, vol. 5, pp. 793-97.
30. D. J. Coates, J. W. Evans, A. L. Cabrera, G. A. Somorjai, and H. Heineman: *J. Catalysis*, 1983, vol. 80, pp. 215-20.
31. D. J. Coates, J. W. Evans, and H. Heinemann: *J. Appl. Catalysis*, 1983, vol. 7, pp. 233-41.
32. T. Gabor and J. M. Blocher: *J. Vac. Sci. Technol.*, 1969, vol. 6, pp. 815-27.
33. M. E. Hall: M. S. Thesis, LBL-18902, Lawrence Berkeley Laboratory, U.C., Berkeley, CA, 1985.
34. H. Hashimoto, S. Urai, H. Yotsumoto, and J. Sawamori: in *Proc. 7th Int. Congr. Electron Microscopy*, Grenoble, 1970, vol. 2, pp. 399-400.
35. H. R. Harrison, R. Aragon, and C. J. Sandberg: *Mat. Res. Bull.*, 1980, vol. 15, pp. 571-80.
36. D. H. St. John, S. P. Matthew, and P. C. Hayes: *Metall. Trans. B*, 1984, vol. 15B, pp. 709-17.
37. D. H. St. John, S. P. Matthew, and P. C. Hayes: *Metall. Trans. B*, 1984, vol. 15B, pp. 701-08.
38. *Bulletin of Alloy Phase Diagrams*, 1980, vol. 1, No. 1, p. 29.
39. E. N. Fuller, P. D. Schettler, and J. C. Giddings: *Indust. and Eng. Chem.*, 1966, vol. 58, pp. 18-27.
40. W. Pluschkell and B. V. S. Sarma: *Arch. Eisenhüttenwes.*, 1974, vol. 45, pp. 23-31.